A "seabird-eye" on mercury stable isotopes and cycling in the Southern Ocean

Marina Renedo, Paco Bustamante, Yves Cherel, Zoyne Pedrero, Emmanuel Tessier, David Amouroux

A “seabird-eye” on mercury stable isotopes and cycling in the Southern Ocean

Marina Renedo[a,b,*], Paco Bustamante[a,c], Yves Cherel[d], Zoyne Pedrero[b], Emmanuel Tessier[b], David Amouroux[b,*]

[a] Littoral Environnement et Sociétés (LIENSs), UMR 7266 CNRS- La Rochelle Université, 2 rue Olympe de Gouges, 17000 La Rochelle, France

[b] Universite de Pau et des Pays de l’Adour, E2S UPPA, CNRS, IPREM, Institut des Sciences Analytiques et de Physico-chimie pour l’Environnement et les matériaux, Pau, France

[c] Institut Universitaire de France (IUF), 1 rue Descartes 75005 Paris, France

[d] Centre d'Etudes Biologiques de Chizé (CEBC), UMR 7372 CNRS-La Rochelle Université, 79360 Villiers-en-Bois, France

**Corresponding authors:* marina.renedo@ird.fr, david.amouroux@univ-pau.fr

Abstract

Since mercury (Hg) biogeochemistry in the Southern Ocean is minimally documented, we investigated Hg stable isotopes in the blood of seabirds breeding at different latitudes in the Antarctic, subantarctic and subtropical zones. Hg isotopic composition was determined in adult penguins (5 species) and skua chicks (2 species) from the Adélie Land (66°39′S, Antarctic) to Crozet Islands (46°25′S, subantarctic) and Amsterdam Island (37°47'S, subtropical). Mass-dependent (MDF, δ^{202}Hg) and mass-independent (MIF, Δ^{199}Hg) Hg isotopic values separated populations geographically. Antarctic seabirds exhibited lower δ^{202}Hg values (-0.02 to 0.79 ‰, min-max) than subantarctic (0.88 to 2.12 ‰) and subtropical (1.44 to 2.37 ‰) seabirds. In contrast, Δ^{199}Hg values varied slightly from Antarctic (1.31 to 1.73 ‰) to subtropical (1.69 to 2.04 ‰) waters. The extent of methylmercury (MeHg) photodemethylation extrapolated from Δ^{199}Hg values was not significantly different between locations, implying that most of the bioaccumulated MeHg was of mesopelagic origin. The larger increase of MDF between the three latitudes co-varies with MeHg concentrations. This supports an increasing effect of specific biogenic Hg pathways from Antarctic to subtropical waters, such as Hg biological transformations and accumulations. This "biogenic effect" among different productive southern oceanic regions can also be related to different mixed layer depth dynamics and biological turnover that specifically influence the vertical transport between the mesopelagic and the photic zones. This study shows the first Hg isotopic data of the Southern Ocean at large scale and reveals how regional Southern Ocean dynamics and productivity control marine MeHg biogeochemistry and the exposure of seabirds to Hg contamination.

Keywords: *methylmercury, biogeochemistry, latitude gradients, penguins, skuas*

Graphical abstract

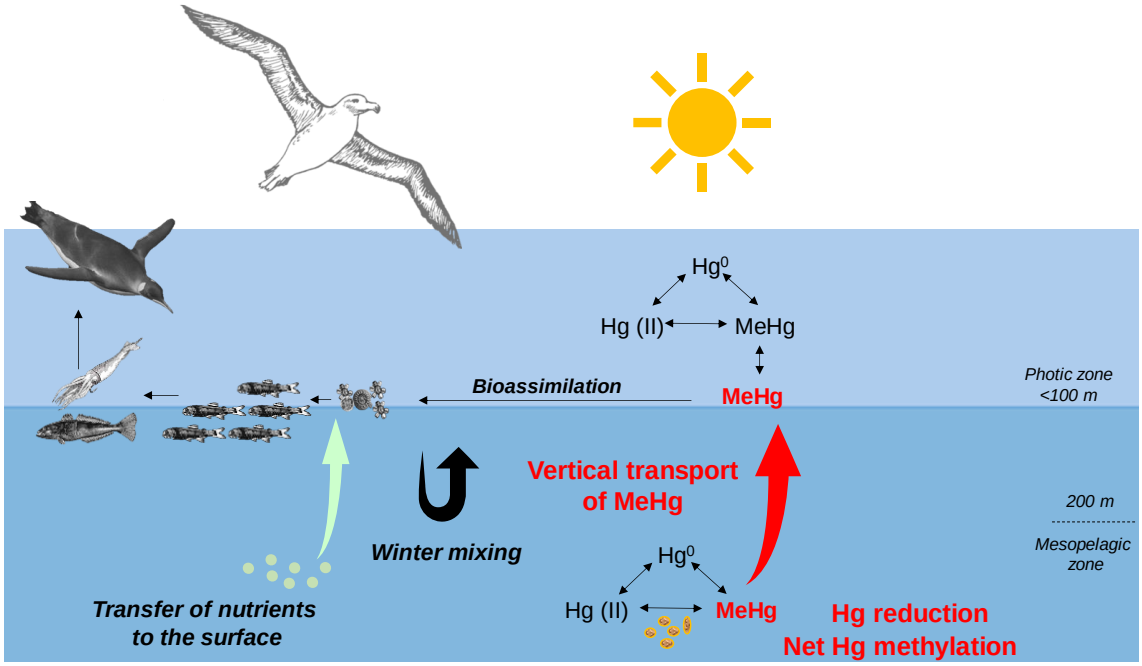

1. Introduction

Although the Southern Ocean is usually perceived as a pristine area untouched by anthropogenic pressures, contaminants can nonetheless reach this region by ocean circulation and atmospheric transport (Fitzgerald et al., 2007). Mercury (Hg) is considered a globally distributed contaminant of major concern for humans and wildlife, especially in its methylmercury (MeHg) form (Eagles-Smith et al., 2018). Indeed, MeHg is a potent organometallic neurotoxin that accumulates in living organisms and that biomagnifies within food webs (Mason et al., 1996; Watras et al., 1998). The Hg biogeochemical cycle is highly complex and comprises several chemical processes and biological transformations, such as methylation/demethylation and redox reactions, that control MeHg production and its bioavailability to marine organisms. Hg methylation is thought to be mainly driven by anaerobic micro-organisms within the water column down to at least the oxygen minimum zone (Lehnherr et al., 2011, Heimbürger et al., 2015). Due to biomagnification processes, top predators are

exposed to high levels of MeHg, thereby presenting severe health risks for their populations (Tartu et al., 2013, Goutte et al., 2014ab).

In the Southern Ocean, particularly in the Indian Ocean sector, various studies have reported significant levels of Hg bioaccumulation in top predators such as seabirds (Carravieri et al., 2014, 2017, 2020; Cherel et al., 2018), with a common MeHg concentration trend exhibiting 4 to 8-fold higher concentrations in Subtropical relative to Antarctic populations for all of the seabird species studied to date (Carravieri et al., 2014, 2017). There is however a paucity of information in regard to Hg concentrations, the spatial distribution, and speciation in the water column from this remote area of the world's oceans (Cossa et al., 2011; Lamborg et al., 2014, Canario et al., 2017). Complex oceanic dynamics along the Southern Ocean regions induce changes in the properties and subduction/upwelling rates of water masses (Sallée et al., 2010), thereby influencing the vertical advection of MeHg in the water column (Cossa et al., 2011), and consequently its availability for its assimilation within the marine food web. Substantial inter-seasonal variations also result in build-up of Hg-enriched surface waters during winter months and its subsequent downward transfer during spring and early summer (Cossa et al., 2011) before the shallow mixed layer is re-established (Sallée et al., 2010).

The study of Cossa et al., (2011) is the only one to date investigating latitudinal variations of methylated Hg (MeHg and dimethylmercury (Me_2Hg)) and the distribution in the water column of the Southern Ocean. This study revealed slightly higher concentrations in Antarctic seawaters (0.15 to 0.21 pmol L^{-1}) compared to Subantarctic and Subtropical seawaters (0.08 to 0.10 pmol L^{-1}). Although these data only reflected a single seasonal setting, this north to south gradient of increasing MeHg concentrations in water is opposite to the trend observed in the tissues of seabirds (Becker et al., 2016; Carravieri et al., 2014, 2017, 2020; Cherel et al., 2018). However, the seasonal mismatch (March-April) between the sampling campaign of Cossa et

al., (2011) and studies during seabird breeding stages (November-February) (Carravieri et al., 2014, 2017, 2020) must be carefully considered because intra-annual fluctuations in vertical oceanic dynamics, atmospheric deposition, chlorophyll-a concentrations, and light irradiance availability could affect MeHg production, transformations and transport in the water column. The spatial range of methylated Hg concentrations (MeHg and Me_2Hg) reported in the Southern Ocean water column might drive variations in biota MeHg concentrations. However, seasonal and geographical differences in Hg atmospheric deposition and Hg release during the melting of sea ice can greatly influence Hg concentrations in the water column. Therefore, Hg assimilation efficiency for primary producers might also be altered, thereby making this association much more complex. For instance, higher productivity in Antarctic and Polar Front zones (Sullivan et al., 1993, Sokolov, 2008), could dilute biologically the MeHg reducing its uptake at the base of the food web (Pickhardt et al., 2002). Additionally, differences in food web complexities between ecosystems (Cherel et al., 2007, Bost et al., 2009), could induce a differential MeHg biomagnification, leading to different levels of exposure in top predators (Lavoie et al., 2013).

The measurement of subtle deviations in naturally occurring Hg stable isotope ratios provides a new and powerful perspective for the exploration of the cycle of this element, and it has been shown to be useful to depict Hg sources or to quantify its reactivity within different environmental compartments (Blum et al., 2014). Hg has seven isotopes that experience mass-dependent and mass-independent isotopic fractionation (MDF and MIF, respectively). Most biogeochemical processes such as volatilization, reduction, absorption, demethylation, and methylation induce MDF (usually reported as $\delta^{202}Hg$) (Kritee et al., 2007, 2009; Rodriguez Gonzalez et al., 2009; Zheng and Hintelmann, 2010). Aqueous photochemical processes (MeHg photodemethylation and inorganic Hg photoreduction) have been shown to lead to significant

levels of MIF of odd Hg isotopes (Δ^{199}Hg and Δ^{201}Hg) (Bergquist and Blum, 2007; Zheng and Hintelmann, 2009; Perrot et al., 2012). Intracellular odd-MIF was recently discovered during photomicrobial MeHg demethylation and Hg(II) reduction in a marine microalga in the presence or absence of UV-B light (Kritee et al., 2017). MIF of even-mass Hg isotopes, reported as Δ^{200}Hg and Δ^{204}Hg (i.e., anomalous fractionation of the $^{200/198}$Hg and $^{204/198}$Hg ratio from the theoretical MDF line), was first detected in rainfall samples and is thought to be associated to mechanisms occurring in the atmosphere, such as photo-oxidation in the upper tropopause and/or neutron capture in space (Gratz et al., 2010; Chen et al., 2012; Cai and Chen, 2015). This signature is increasingly being investigated as a potential tracer of Hg sources of atmospheric origin. Consequently, the combination of Hg MDF and MIF signatures provide interesting and complementary information for potential sources and transformation pathways of Hg. In the Southern Ocean, Hg isotopic investigations in sediments and biota are limited to the Antarctic sector (Zheng et al., 2015; Liu et al., 2019), and as a result, the information about the biogeochemical cycle of Hg in larger zones across Antarctic remote oceanic regions remains insufficient (Bowman et al., 2020).

Seabirds are meso- to top- predators that forage in various compartments of the pelagic ecosystems. Several studies have demonstrated the usefulness of seabirds to assess Hg contamination as far as the biological characteristics are mastered (e.g. moulting patterns, migration or foraging strategies (Furness and Camphuysen, 1997; Carravieri et al., 2013, 2016; Bustamante et al., 2016). Chicks of flying birds and both chick and adult penguins (a group of diving birds) are the most pertinent seabird models for tracing local Hg contamination pathways using Hg isotopic approaches because they reflect the Hg contamination around the colony (Blévin et al., 2013; Renedo et al., 2018a). Previous studies extensively explored the physiological, ecological and environmental aspects concerning the specific application of skua

chicks and adult penguins for effective biomonitoring of Hg contamination at a large scale of the Southern Ocean (Carravieri et al., 2016, 2017). Therefore, the use of skua chicks and adult penguins for Hg isotopic investigations provides significant advantages in regard to the survey of Hg sources and its associated biogeochemical processes in the ocean (Point et al., 2011; Day et al., 2012; Zheng et al., 2015; Renedo et al., 2018b). Moreover, non-lethal sampling of feathers (reflecting the inter-moult period) and blood (reflecting short-term exposure) provides complementary and specific spatio-temporal information of Hg exposure in adults (Renedo et al., 2018a). Since blood Hg reflects recent Hg acquisition over the last weeks preceding sampling (Bearhop et al., 2000), the Hg isotopic composition of blood of chicks and penguins is considered as indicative of local exposure with a relevant resolution (Renedo et al., 2018a). In this work, we investigated the Hg isotopic composition (mainly as MeHg; Renedo et al., 2018a) of blood cells of two seabird models (skua chicks and adult penguins) in Antarctic, Subantartic and Subtropical zones (Fig. 1). We hypothesized that the specific regional MeHg dynamics and transfer to the marine pelagic trophic chain at different latitudes of the Southern Indian Ocean could lead to significant variations of Hg isotopic signatures of seabird blood (both MIF and MDF), then providing new insights to better constrain Hg and MeHg cycling in the Southern Ocean and seabird exposure to Hg.

2. Material and Methods

2.1. Sample collection and sampling sites. Blood samples were collected during the Austral summer 2011-2012 (from October to February) at the four sites of the Terres Australes et Antarctiques Françaises, from south to north: the high-Antarctic Adélie Land (66°40’S, 140°10’E), Subantarctic Kerguelen (49°21′S, 70°18′E) and Crozet Islands (46°26’S, 51°45’E), and the Subtropical Amsterdam Island (37°50’S, 77°31’E). Chicks from two species of skuas (the south polar skua *Catharacta maccormicki* in Adélie Land and the brown skua *C. lonnbergi*

elsewhere) and adults from five species of penguins (king penguin *Aptenodytes patagonicus*, Adélie *Pygoscelis adeliae*, macaroni *Eudyptes chrysolophus*, eastern rockhopper *E. chrysocome filholi* and northern rockhopper *E. chrysocome moseleyi*) were randomly chosen at the end of the chick-rearing period (Fig. 1). Blood was sampled from an alar vein, centrifuged to separate the plasma from the blood cells (hereafter blood) which were kept frozen at −20 °C. Before the analysis, blood samples were lyophilized with Hg concentrations being reported as dry weight (dw). The dates and localities of the sampling protocol, as well as the ecological characteristics of each seabird species at the various localities are specified in the SI section. Carbon ($\delta^{13}C$) and nitrogen ($\delta^{15}N$) stable isotope ratios were determined in blood cells as detailed in previous work (Renedo et al., 2018b).

2.2. Reference materials, sample preparation, and analytical description

Reference samples. To validate the analytical results for Hg speciation, four certified reference materials were analyzed: human hair NIES-13 and IAEA-086; tuna fish ERM-CE-464 and dogfish liver DOLT-4 (Table S1). Hg isotopic results for blood were also validated with these four reference materials by intercomparison with previously reported values (Li et al., 2014; Yamakawa et al., 2016) and with reference values of Lake Michigan fish tissue NIST SRM 1947. Two internal reference samples were also prepared with the pooled samples collected from different king penguin individuals from Crozet Islands: RBC-KP (red blood cells) and F-KP (feathers) and were analyzed at each analytical session. Analytical uncertainty for delta values was calculated using SD typical errors for reference materials, as recommended by reference publications for standard reporting of Hg isotopic ratio uncertainties (Table S2).

Measurement of the Hg compound concentrations (GC-ICPMS). For speciation analyses, Hg was extracted from blood (0.10-0.15 g) by alkaline microwave digestion with 5 mL of

tetramethylammonium hydroxide (25% TMAH in H_2O, Sigma Aldrich) (Rodrigues et al., 2011; Queipo Abad et al., 2017). The extraction method, analysis, and quantification of Hg species have been detailed previously (Renedo et al., 2018a). Total Hg concentrations were quantified by using an advanced Hg analyzer (AMA-254, Altec). Total Hg concentrations obtained by Hg speciation analyses (i.e., the sum of inorganic and organic Hg) were compared to total Hg concentrations obtained by AMA-254 for method validation. Recoveries of Hg and MeHg concentrations with respect to certified values for each reference material varied between 96 and 101% (see Table S1 for details).

Measurement of the total Hg isotopic composition by CVG-MC-ICPMS. For isotopic analyses, blood (0.05-0.10 g) was predigested overnight at room temperature and then digested the following day with 3 or 5 mL of HNO_3 acid (65%, INSTRA quality). Samples were subsequently extracted in a Hotblock at 75 ºC for 8 h (6 h in HNO_3 and >2 h after the addition of 1/3 of the total volume of H_2O_2 (30%, ULTREX quality)). Hg isotopic analyses were carried out as reported previously (Renedo et al., 2018a). Hg isotopic values were reported as delta notation, calculated relative to the bracketing standard NIST SRM-3133 reference material to allow inter-laboratory comparisons, as described in the SI section. NIST SRM-997 thallium standard solution was used for the instrumental mass-bias correction using the exponential law. Secondary standard NIST RM-8160 (previously UM-Almadén standard) was used for validation of the analytical session (Table S2). Total Hg concentrations in the extract solution were compared to the concentrations found by AMA-254 analyses to assess method recovery. The obtained average recovery was 100 ± 2% (n=110).

2.3. Statistical tests

Statistical analyses were performed using R 3.3.2 software (R Core Team, 2016). Prior to the analyses, the data were checked for normality of the distribution and homogeneity of variances using Shapiro–Wilk and Breusch-Pagan tests, respectively. Non-parametric tests (Kruskal–Wallis with the Conover-Iman test) were performed accordingly. We examined the correlations between MeHg concentrations, Hg MDF (δ^{202}Hg) and MIF (Δ^{199}Hg and Δ^{200}Hg) with latitude using linear regressions and Spearman correlation rank tests. Statistically significant results were set at $\alpha = 0.05$.

3. Results and discussion

3.1. Total Hg concentrations (THg) and Hg speciation trends

MeHg was the dominant Hg form in the blood of all the individuals (92 ± 7%, mean ± SD; Table 1). This means that Hg isotopic composition of blood corresponded essentially to the MeHg isotopic values. Both the skua and penguin blood samples exhibited significantly different MeHg concentrations according to the sites (Kruskal-Wallis, H=31.09 and 43.05, respectively, both $p < 0.0001$). The skua blood MeHg concentrations increased from 0.51 to 3.78 $\mu g \cdot g^{-1}$ dw (n=40) from the Antarctic to Subtropical populations, respectively. Concentrations of MeHg in penguin blood were also lower for Antarctic than for Subtropical species (0.43 to 1.95 $\mu g \cdot g^{-1}$ dw, respectively, n=51), increasing in the order Adélie < eastern rockhopper < macaroni < king < northern rockhopper penguins (Table 1). MeHg concentrations in seabird blood showed a significant correlation with latitude for both skuas (Adjusted r^2=0.62, $p<0.0001$) and penguins (Adjusted r^2=0.33, $p<0.0001$) (Fig. S1). Previous studies addressed the influence of the intrinsic and extrinsic ecological factors of these two seabird models (age, sex, moulting patterns, diet or feeding habitats) on the latitudinal variations

of MeHg concentrations (Carravieri et al., 2016, 2017), as well as the Hg isotopic composition (Renedo et al., 2018a) of blood or feathers at the same study sites. The main factor explaining inter-species differences in Hg levels in a same ecosystem were feeding habits, rather than physiological or taxonomic differences (Carravieri et al., 2014, 2016). However, the influence of the dietary habits did not influence the latitudinal variations of MeHg blood levels, suggesting that the higher seabird MeHg concentrations in Subtropics than in Antarctica depend mainly on the geographical differences of Hg sources and dynamics (Renedo et al., 2018b) or incorporation into food webs (Carravieri et al., 2016).

3.2. Latitudinal trends of Hg stable isotopic composition

A wide range of mean blood δ^{202}Hg values was observed between Antarctic and Subtropical populations for both skuas and penguins (0.23-1.56 ‰ and 0.53-2.16 ‰, respectively) (Table 1). The mean variation of δ^{202}Hg values of blood between Antarctic and Subtropical sites was 1.33 ± 0.15 ‰ (-0.02 to 1.71 ‰) for skuas and 1.60 ± 0.25 ‰ (0.24-2.37 ‰) for penguins. We observed a significant relationship between latitude and δ^{202}Hg values of blood for skuas and penguins (Adjusted r^2=0.90 and 0.85, respectively, both $p < 0.0001$) (Fig. 2A). Δ^{199}Hg values varied slightly between the various sites in skuas (1.51-1.76 ‰) and penguins (1.54-1.89 ‰). The mean variation of Δ^{199}Hg values was 0.25 ± 0.09 ‰ (1.31-1.85 ‰) for skuas and 0.36 ± 0.16 ‰ (1.38-2.04 ‰) for penguins. The Δ^{199}Hg values of blood were also significantly correlated with latitude in skuas (Adj. r^2=0.55, $p < 0.0001$) and penguins (Adj. r^2=0.18, $p<0.0001$) (Fig. 2B). Low differences were observed for the even-MIF signatures (denoted here as Δ^{200}Hg) between Antarctic (-0.02 ± 0.04 ‰) and Subtropical populations (0.04 ± 0.05 ‰). The even-MIF values of Subantarctic seabirds (0.00 ± 0.04 ‰) were not significantly different from Antarctic seabirds, when skuas and penguins were considered together (H=13.22, p=0.001). Although the even-MIF latitudinal variations were low for the two groups of seabirds,

they exhibited a significant linear trend with latitude in both skuas (Adj. r^2=0.15, p=0.008) and penguins (Adj. r^2=0.15, p=0.001) (Fig. 2C).

The strong relationship of Hg isotopic signatures with latitude (Fig. 2) could be explained by a combined influence of different Hg sources (with different Hg isotopic baselines) and processes associated with geographically changing conditions that would induce Hg isotopic fractionation across the study sites. In the following sections, we conceptually propose, estimate and discuss the contribution of these potential explanatory factors, from regional atmospheric sources (even Hg-MIF), through sea surface photochemistry (Hg odd-MIF) to biotic dark processes in the water column (additional Hg MDF).

3.3. Regional atmospheric sources potentially affect Hg isotopic baseline in seabirds from distant latitudes of the Southern Ocean

Hg even-MIF (Δ^{200}Hg) is thought to be associated with mechanisms occurring in the upper atmosphere, and it is not affected by any biogeochemical processes, including photochemical processes in the euphotic zone, as observed so far (Gratz et al., 2010; Chen et al., 2012; Sherman et al., 2012). The Δ^{200}Hg values detected in the blood of skuas and penguins exhibited minor variations between the distant latitudes and high variability at the population level (Fig. 2C). We observed higher Δ^{200}Hg values in Subtropical seabirds (skuas + penguins) from Amsterdam Island (0.04 ± 0.05‰), whereas slightly lower Δ^{200}Hg values were obtained in Subantarctic (0.00 ± 0.04‰) and Antarctic seabirds (-0.02 ± 0.04‰). Our Δ^{200}Hg values of seabirds are in the same range to the observed in Arctic marine predators of Alaska that also presented a decreasing trend of Δ^{200}Hg values with latitude (from 0.10 to -0.01‰; 53.93 to 71.30°N, Masbou et al., 2018). Interestingly, precipitation samples worldwide generally exhibited an inverse latitudinal gradient, with higher Δ^{200}Hg values at high latitudes relative to low latitude regions (Chen et al., 2012; Gratz et al., 2010; Sherman et al., 2012b), which is potentially

associated with the shallower troposphere at higher latitudes (Cai and Chen, 2015). The inversed Δ^{200}Hg trends between atmospheric samples and biological tissues with latitude highlights the complexity of Hg atmospheric deposition pathways and the necessity of further research exploring Hg isotopes in atmospheric samples in Southern Polar Regions to elucidate the mixed contribution of Hg atmospheric inputs. Although the slight variations of seabird Δ^{200}Hg values do not provide conclusive evidence, our close-to-zero data is closer to the values observed atmospheric total gaseous Hg (−0.11 to −0.01‰, Demers et al., 2013; Sherman et al., 2010). This seems to indicate that the predominant Hg atmospheric source are originating from tropospheric gaseous elemental Hg, which would be oxidized to Hg^{2+} and deposited as dry or wet deposition, and eventually re-emitted after reduction in surface environment. Recent models in the Arctic Ocean estimated limited uptake of Hg^0 as a result of ice cover and saturation of surface waters in dissolved Hg^0 (Soerensen et al., 2016), therefore analogous processes in sea-ice covered regions of Antarctica can be assumed. Though, the sequestration of atmospheric Hg^0 (and oxidized Hg^{2+}) in the sea ice compartment in Antarctic zones is thought to be responsible for an additional input of Hg to the ocean (Cossa et al., 2011; Gionfriddo et al., 2016). Moreover, additional processes could transport oxidized Hg^{2+} from the Antarctic continent to Antarctic coasts by katabatic winds (Angot et al., 2016), also contributing to negative Δ^{200}Hg values registered in Antarctic seabird populations. Arctic snowfall impacted by atmospheric depletion events exhibited mostly negative to near-to zero Δ^{200}Hg values (-0.12‰, Sherman et al., 2010), therefore we suggest that substantial deposition of oxidized Hg^{2+} in the Antarctic snowpack and consequent melting of ice could contribute to negative Δ^{200}Hg values in the Antarctic ecosystem. Slightly negative Δ^{200}Hg values in Antarctic ornithogenic sediments (down to -0.07 ‰, Zheng et al., 2015) are also close to the relatively negative values registered in our Antarctic seabirds. Indeed, sediment erosion and its mobilization to opened areas could also contribute to Hg release into the aquatic compartment in water masses

surrounding the Antarctic continent or the coastal zones in the vicinity of the Subantarctic islands. On the assumption that a higher interaction between coastal sediment and biota is produced in the Antarctic zone near the continent compared to Subantarctic and Subtropical islands, Δ^{200}Hg values in Antarctic seabirds breeding in Adélie Land may be also lower relative to Subantarctic and Subtropical communities. However, sediment Hg inputs in coastal waters of the Subantarctic and Subtropical islands are not negligible, since Hg isotopes from the coastal and partly benthic gentoo penguin *Pygoscelis papua* are influenced by sediment-derived Hg at the local scale of the Crozet archipelago (Renedo et al., 2018b).

3.4. Low variability of MeHg photodemethylation extent between distant latitudes of the Southern Ocean

As a significantly positive Hg odd-MIF is thought to be mainly due to the photochemical processes prior to MeHg incorporation into food webs (Bergquist and Blum, 2007), we initially considered that the variability of Δ^{199}Hg values of seabirds between the three geographically distant areas (Antarctic, Subantarctic, and Subtropical) (Fig. 2B) could be primarily due to distinct conditions influencing photochemical reactivity in surface waters. Aquatic photochemical MeHg demethylation is known to induce an increase in odd-MIF (Δ^{199}Hg and Δ^{201}Hg) and in MDF values (δ^{202}Hg) in the residual MeHg pool (Bergquist and Blum, 2007). This process results in a Δ^{199}Hg/Δ^{201}Hg ratio of 1.36 ± 0.04, as reported experimentally (Bergquist and Blum, 2007). Meanwhile, experimental photochemical reduction of Hg(II) yielded a Δ^{199}Hg/Δ^{201}Hg ratio of 1.00 ± 0.01 (Bergquist and Blum, 2007). The Δ^{199}Hg/Δ^{201}Hg slopes obtained for penguin blood (1.17 ± 0.06, intercept: -0.07 ± 0.08, SE) and skua blood (1.14 ± 0.07, intercept: 0.05 ± 0.11, SE) (Fig. S2) differed slightly from those obtained from previous photodemethylation laboratory experiments, but they are in good agreement with those previously obtained with marine fish (Senn et al., 2010; Blum et al., 2013) and seabird

eggs (Point et al., 2011; Day et al., 2012). The overall $\Delta^{199}Hg/\Delta^{201}Hg$ slope for both skuas and penguins was 1.16 ± 0.05 (SE) with negligible intercept (0.01 ± 0.07). Our slopes were also similar to the $\Delta^{199}Hg/\Delta^{201}Hg$ ratios obtained in fish from King George Island (1.19 ± 0.17, n=8; Liu et al., 2019) and faeces from Antarctic seals (1.16, n=2; Zheng et al., 2015), but slightly lower than ratios reported on Adélie penguin guano (~1.30, n=2; Zheng et al., 2015). The lower $\Delta^{199}Hg/\Delta^{201}Hg$ slopes typically observed in marine biota compared to laboratory photochemical experiments can be the consequence of differences in organic matter or the influence of dissolved cations and halogens present in seawater. Recently, other studies have focused on the influence of the type of solar radiation and different ligands in MeHg photodemethylation processes in aquatic systems (Chandan et al., 2015; Rose et al., 2015). Rose et al., (2015) investigated the effect of solar radiation (different intensities and frequencies) on Hg MIF during MeHg aquatic photodemethylation and obtained a ratio similar to Bergquist and Blum (2007). Chandan et al., (2015) documented variable $\Delta^{199}Hg/\Delta^{201}Hg$ ratios for MeHg photodemethylation under different types and concentrations of dissolved organic carbon (DOC) ligands with different content of reduced sulphur (S-red). Under low MeHg/S-red-DOC ratios $\Delta^{199}Hg/\Delta^{201}Hg$ slopes were consistent and less variable (1.38±0.02); whereas high MeHg/S-red-DOC ratios presented lower slopes varying from 1.17±0.04 to 1.30±0.02 (Chandan et al., 2015).

Assuming that MeHg photodegradation is the dominant photochemical process before MeHg incorporation into food webs, we estimated the fraction of photodemethylated MeHg of each area based on three experimental models (Bergquist and Blum, 2007; Chandan et al., 2015). Although the use of experimental models based on more realistic environmental conditions (low MeHg: Sred-DOC ratios) can be more representative of the processes occurring under natural conditions in the environment, we are conscious of the degree of extrapolation of these

models to real environments. Therefore, the isotopic fractionation systems of these models were adjusted to our specific conditions of MeHg:Sred-DOC ratios and MeHg:DOC ratios by fitting equations for the three sites (Antarctic, Subantarctic and Subtropical zones) to maximize the accuracy and veracity of our estimations (Tables S5, S6 and S7). The difference in the extent of photodemethylated MeHg from Antarctic and Subantarctic to Subtropical zones was on the order of 2%, independently of the experimental model used. Taking the closer estimates for MeHg, DOC, and dissolved organic sulfur (DOS) concentrations in the study areas (Bergquist and Blum, 2007; Chandan et al., 2015), the extent of photodemethylated MeHg varied from ~ 9% in Antarctic to ~ 11% in Subtropical zones (Table S8). Despite the wide distance between the studied sites, the variation of the extent of MeHg photodemethylation was surprisingly low. For instance, previous isotopic investigations in open ocean areas reported an extent of MeHg photodemethylation of ~40-80% (Senn et al., 2010; Blum et al., 2013), although the high degree of stratification and low productivity of these oligotrophic opened areas compared to our studied sector of the Southern Ocean can lead to this significant difference. However, our estimated MeHg photodemethylation extents are similar to those calculated in eggs of seabirds of the Arctic Ocean (~8-16%, Point et al., 2011) and in ornithogenic sediment cores of the Antarctic coastal ecosystem (~13-18%; Zheng et al., 2015), using similar calculation models (Chandan et al., 2015). A similar variation of the degree of MeHg photodemethylation was also calculated across the Crozet penguin community between benthic (13%) and epipelagic (16%) foragers (Renedo et al., 2018b) also estimated using similar calculation models (Bergquist and Blum, 2007; Chandan et al., 2015). Also, Blum et al., (2013) found that the fish Δ^{199}Hg values of the MeHg in mesopelagic fish of the Pacific Ocean were about 1.5 - 2.0 ‰., i.e. within the same range as Δ^{199}Hg values for seabirds in our study.

Based on the previous observations of Hg isotopes of penguins from Crozet Islands (Renedo et al., 2018b) and on the variations observed of Hg odd-MIF as a function of the foraging depth of marine fish (Blum et al., 2013), the low degree and the minor variations of MeHg photodegradation in distant sites of the Southern Ocean strongly suggest that the major proportion of the MeHg that accumulated in the seabirds was minimally photodemethylated, thus primarily originating from dark environments. Moreover, maximum MeHg concentrations in the open ocean water column are commonly observed at areas with minimum oxygen levels (Monperrus et al., 2007; Kirk et al., 2008; Sunderland et al., 2009; Cossa et al., 2009), including in the Southern Ocean (Cossa et al., 2011). These observations demonstrated active MeHg production and accumulation in organisms from such environments (e.g., Chouvelon et al., 2012). Substantial deep net Hg methylation can be supported by a larger export of organic matter (Sokolov, 2008; Sullivan et al., 1993), subsequent larger inorganic Hg substrate supply (Cossa et al., 2011) from the euphotic zone (< 60 m depth; Tripathy et al., 2015) to mesopelagic waters, and MeHg preservation from photodegradation (Monperrus et al., 2007; Heimbürger et al., 2015). Therefore, the existence of substantial net methylation occurring at depth suggests that the MeHg accumulated in seabirds from the Southern Ocean was predominantly of mesopelagic origin. Further, the lower $\Delta^{199}Hg/\Delta^{201}Hg$ slopes of seabirds compared to previous studies (i.e. Blum et al., 2013) also suggest potential export of surface Hg^{2+} to mesopelagic environments where it is methylated. Due to the high intensity of winter cooling and the seasonal mixed layer depths oscillations, the vertical transport of MeHg and Hg^{2+} between shallow and deep-water masses could be a preponderant factor explaining the low extent of photochemical processes over these oceanic regions.

3.5. Major variations of the Hg isotopic composition between distant latitudes indicate distinct regional biogenic transformation and bioaccumulation extent.

Trophic transfer and accumulation. The strong correlation between the Δ^{199}Hg and the δ^{202}Hg values of both skuas and penguins (Adj. r^2=0.76 and 0.61, respectively, both $p< 0.0001$; Fig. S3) could be indicative of different sources of Hg with distinct isotopic signatures (MDF and MIF) and/or different processes before Hg incorporation or during uptake and bioaccumulation in the food web that produce both Hg MDF and MIF across the different sites. By calculation of the corresponding latitudinal differences of δ^{202}Hg obtained experimentally for photochemical demethylation (Chandan et al., 2015), we estimated that approximately 0.3 ‰ of the total δ^{202}Hg variation may be induced by photochemical MeHg breakdown (Tables S9 and S10). This means that the remaining 1.0-1.3 ‰ of δ^{202}Hg differences between latitudes may be the consequence of various Hg sources and/or biogeochemical processes inducing a reservoir of isotopically heavier Hg in the Subtropical region (Fig. 3).

The Antarctic ecosystem is characterized by a less complex food web in which top predators feed mainly on a limited number of key available species, such as the Antarctic krill *Euphausia superba* (Cherel, 2008; Brasso et al., 2014). By contrast, Subantarctic and Subtropical ecosystems have a larger diversity of prey species including four species of Euphausiids (Cherel et al., 2007; Bost et al., 2009), constituting more complex food webs. Therefore, the difference in food web complexity between the studied sites could explain the increasing MeHg levels from Antarctic to Subtropical ecosystems (Lavoie et al., 2013). However, such difference in the marine trophic transfer of MeHg was not yet found to induce any significant variations of δ^{202}Hg. Trophic processes do not appear to explain the total MDF variation, because both seabird models with contrasting trophic ecologies exhibited the same MDF variations between the different latitudes and similar associated slopes. Indeed, although higher blood Hg

concentrations were obtained in skua chicks relative to adult penguins at each locality, skuas exhibited lower δ^{202}Hg values despite their higher trophic level (Carravieri et al., 2014). Since the two different seabird species have contrasted foraging ecology, different MDF values would be expected due to distinct foraging habitats, trophic levels, and consequently different level of exposure to MeHg, Different extent of metabolic processes due to both age status and species-specific characteristics can also lead to significant MDF variations among seabirds. The lower MDF values in seabird chicks could be therefore potentially explained if metabolic processes are less efficient due to their age. This would induce lower *in vivo* Hg isotopic fractionation, thereby leading to lower blood δ^{202}Hg values compared to adult penguins. To check this hypothesis, we investigated skua adult blood from the Kerguelen population, for which significantly higher δ^{202}Hg values (a mean ~0.54 ‰ difference) were observed compared to chicks, and which also matched with the penguins' MDF-latitude slope (Fig. S4). This observation suggested that the difference in δ^{202}Hg values between the two models may be due to a specific metabolic response related to age and/or species, while the latitudinal variation remains mostly independent of such internal biotic pathways. This conclusion agrees with those of previous studies in marine fish (Kwon et al., 2012; Blum et al., 2013) in which trophic effects were found to be independent of Hg isotopic trends and did not significantly affect Hg MDF. Variations in δ^{202}Hg values between seabird species of the same ecosystem can be dependent on the Hg sources associated with different integration times between tissues (Renedo et al., 2018a) or specific foraging ecologies (Renedo et al., 2018b). However, the consistent variations of seabird MDF signatures between the different latitudes suggests that a process driven by kinetic isotope fractionation operating at large/regional scales could be the main driver of Hg isotopic geographical variations. In light of this, we have proposed and tested several potential major biogeochemical processes that could drive the observed variations of Hg MDF in seabirds from the four sites (Fig. 4).

Biotic reduction and volatilization. First, we postulated that the higher surface temperature of Subtropical seawaters compared to Antarctic waters could result in a greater degree of biotic reduction and volatilization of inorganic Hg^0 from the aquatic compartment to the atmosphere, thereby leading to a residual pool of isotopically heavier Hg(II) in the aqueous phase. To test this hypothesis, previous experimental results were used to estimate the variation in the extent of Hg volatilization and Hg biotic reduction from Antarctic to Subtropical waters. By considering the specific conditions of water temperature recorded on the approximate latitudinal sites (Cossa et al., 2011; Canario et al., 2017;) and calculation of Henry's law constant reported by experimental studies in seawater (Andersson et al., 2008), we estimated that volatilization can only contribute to 0.03 ‰ of the MDF variation (Table S11). Thus, a different degree of volatilization itself is not enough to explain the total Hg MDF variations across the investigated latitudinal gradient. Based on experimental models for Hg dark bacterial reduction (Kritee et al., 2007, 2008), estimations showed that the extent of biological reduction in Subtropical waters should be on the order of 1.5 to 3 times higher than in Antarctic waters during the summer period to explain the observed MDF variations between regions (Table S12). However, such a high degree of variation in the dark biological reduction rate in the studied oceanic regions should be taken with caution since it cannot be demonstrated by any robust dataset in these regions of the Southern Ocean. Since most of the MeHg that bioaccumulates in seabird tissues seems to originate from the mesopelagic zone (see above), Hg(II) dark biological reduction cannot be discarded, while the environmental conditions are also supposed to be favorable to the formation of MeHg (Sullivan et al., 1993; Cossa et al., 2011). Moreover, we cannot rule out that δ^{202}Hg of MeHg would follow a similar trend after various methylation and demethylation steps.

Biotic net Hg methylation and uptake. As a second hypothesis, we postulated that higher MeHg concentrations in Subtropical seabirds could possibly be the result of greater net biotic methylation taking place in the mesopelagic zone. We refer here as "net" methylation extent to the combination of simultaneous methylation and demethylation processes. An increase in the methylation/demethylation ratio from Antarctic to Subtropical zones could also be in agreement with the isotopically heavier residual pool of $MeHg^{+}$ (i.e., assuming a steady state) in Subtropical zones. Based on experimental measurements of Hg isotopic fractionation during net MeHg methylation under abiotic (Jiménez-Moreno et al., 2013) and biotic (Perrot et al., 2015) conditions, the net degree of methylation should be on the order of 1.5 to 2.5 times higher in Subtropical waters compared to Antarctic waters (Table S13). Although estimates are based on closed system experiments, it is assumed to be equivalent to the processes occurring in diffusion-limited microenvironments within an open system such as the open ocean. The theoretical magnitude of MDF enrichment during net methylation could thus largely explain the observed MDF latitudinal variation across the studied areas. Indeed, potentially increasing net methylation rates from Antarctic to Subtropical zones are very much in line with both the Hg isotopic latitudinal trends and the higher MeHg levels found in Subtropical seabirds compared to those from Antarctica. Latitudinal variations of MeHg concentrations and Hg isotopic signatures of seabird blood are likely the result of spatial differences in the MeHg production and degradation rates, especially in the darker mesopelagic zone, as suggested by the degree of Hg odd-MIF.

Due to the complex processes of MeHg production and bioaccumulation, the correlation between abiotic MeHg concentrations in seawater and MeHg levels in biota is rarely found in marine ecosystems. The existence of clearly distinct bioregions in the Southern Ocean in terms of vertical profiles of phytoplanktonic biomass and the seasonality of bloom timing is closely

related to seasonal fluctuations in vertical oceanic dynamics and light irradiance availability (Ardyna et al., 2017). These factors would clearly affect MeHg production and transport in the water column. Recent Hg isotopic investigations in the North Pacific Subtropical Gyre highlighted that the bioaccumulation of MeHg is strongly linked to the vertical mobilization of Hg with marine sinking particles and by vertical migration of zooplankton (Motta et al., 2019). In the Southern Ocean, an increasing delay in phytoplankton blooms occurs from Subtropical (October) to Subantarctic latitudes (November/December) to Antarctic latitudes (January/February) (Ardyna et al., 2017). Since the bloom periods at each site occurred before or during our sample collection periods during the Austral summer of 2011-2012 (Table S14), the MeHg integration time in seabird blood corresponded to the stage of maximal primary productivity at each sampling site. The seasonal release of nutrients and algal blooms during austral summer (Sullivan et al., 1993; Sokolov and Rintoul, 2007), enhanced by sea-ice melting in Antarctic coastal zones (Sokolov and Rintoul, 2007; Riaux-Gobin et al., 2013), induce a higher productivity in Antarctic and Polar Front zones. This biomass dilution of Hg could then contribute to lower Hg levels accumulated in Antarctic final predators.

Latitudinal and regional differences in the seasonal dynamics and the oceanic vertical exchange of water masses have been observed in the upwelling branch of the Southern Ocean (Marshall and Speer, 2012) . The seasonal variability of the mixed layer depth is substantial in all the sectors of the Southern Ocean (Sallée et al., 2010). During summertime, the mixed layer depth in the vicinity of the Antarctic Circumpolar Current (ACC) reaches about 100 m (Sallée et al., 2010). The water column is destabilized during winter cooling and the mixed layer deepens, finding its maxima at the north of the Antarctic Circumpolar Current, where the amplitude of the seasonal cycle can exceed 400 m, particularly in the Indian sector (Sallée et al., 2010). We therefore suggest, as illustrated in Fig. 4, that these regional dynamics could be potential key

factors influencing the efficiency of the vertical transport of MeHg between deeper mesopelagic waters and surface waters within the euphotic zone (Cossa et al., 2011; Sallée et al., 2010). Deeper mixed layer depths in the north of the Antarctic Circumpolar Current compared to Antarctic waters indicate weaker stratification and deeper vertical mixing at northern Subtropical waters. A shallower winter vertical mixing at Antarctic and Subantarctic waters near the Polar Front could inhibit the downward transport of Hg to deeper pelagic zones, where net methylation should take place. This would also restrain the upward transfer of nutrients and newly formed MeHg at depth and reduce its uptake by phytoplankton and accumulation along the food web. By contrast, a deeper winter mixed layer depth and higher vertical advection to the surface in Subtropical waters should provide efficient downward transport of Hg and subsequent upward transfer of nutrients and MeHg to the productive euphotic zone. As a result, a complex interplay between MeHg formation at depth and winter mixed layer dynamics may contribute to more efficient vertical MeHg upload in Subtropical waters compared to Subantarctic and Antarctic waters. The higher MeHg exposure observed in Subtropical seabirds may, therefore, be the consequence of both greater microbial formation of MeHg and its vertical transport towards the plankton biomass in Subtropical productive zones.

4. Conclusion

The deductions listed above lead to the conclusion that the variability of Hg isotopic signatures among Antarctic to Subtropical seabirds are strongly influenced by both the specific oceanic dynamics and biological productivity turnover from the three contrasted bioregions of the Southern Ocean. Slight variability of Hg odd-MIF isotopic signatures (Δ^{199}Hg) between Antarctic and Subtropical seabirds strongly suggests that the MeHg accumulated in trophic webs from the Southern Ocean has a dominant mesopelagic origin. Significant variability of MDF Hg isotopic signatures (δ^{202}Hg) and its correlation to MeHg concentrations in seabirds

from the three studied latitudes demonstrates how regional Southern Ocean dynamics and productivity control marine MeHg biogeochemistry and the exposure of seabirds to Hg contamination. Indeed, the investigation of δ^{202}Hg latitudinal variability help elucidate the observed increasing MeHg exposure of seabirds from Antarctic to Subtropical waters by an increasing effect of specific biogenic Hg pathways from Antarctic to Subtropical waters, such as Hg biological transformations and accumulation. This study is the first large scale report of Hg isotopic composition in marine organisms from the Southern Ocean and highlights the potential of seabirds to cover for the first time these wide geographic ranges to document Hg isotopic variations at the ocean scale. However, complementary Hg isotopic studies in these isolated regions are essential to deeply understand the processes driving Hg isotope variations in these ecosystems.

Acknowledgements

The authors wish to thank the fieldworkers who helped collecting blood samples. This study received financial and logistical support from the Institut Polaire Français Paul Emile Victor (IPEV, program no. 109, H. Weimerskirch), the French Southern and Antarctic Lands, and by the Agence Nationale de la Recherche (ANR, program POLARTOP, O. Chastel). Special thanks are due to A. Carravieri who managed the sample database. We also wish to thank Prof. S. Blain (UPMC) for fruitful discussions and help with the oceanographic interpretation of our data. The present work was supported financially by the Région Poitou-Charentes (now the Région Nouvelle Aquitaine) through a Ph.D. scholarship to MR, and by the French national program EC2CO Biohefect/Ecodyn//Dril/MicrobiEen (TIMOTAAF project, P.I. D. Amouroux). The IUF (Institut Universitaire de France) is also acknowledged for its support to PB as a senior member.

References

Andersson, M.E., Gårdfeldt, K., Wängberg, I., Strömberg, D., 2008. Determination of Henry's law constant for elemental mercury. Chemosphere 73, 587–592. https://doi.org/10.1016/j.chemosphere.2008.05.067

Angot, H., Dion, I., Vogel, N., Legrand, M., Magand, O., Dommergue, A., 2016. Multi-year record of atmospheric mercury at Dumont d'Urville, East Antarctic coast: Continental outflow and oceanic influences. Atmos. Chem. Phys. 16, 8265–8279. https://doi.org/10.5194/acp-16-8265-2016

Ardyna, M., Claustre, H., Sallée, J., Ovidio, F.D., Gentili, B., Dijken, G., Ortenzio, F.D., Arrigo, K.R., 2017. Delineating environmental control of phytoplankton biomass and phenology in the Southern Ocean 5016–5024. https://doi.org/10.1002/2016GL072428

Bearhop, S., Ruxton, G.D., Furness, R.W., 2000. Dynamics of mercury in blood and feathers of greet skuas. Environ. Toxicol. Chem. 19, 1638–1643. https://doi.org/Doi 10.1897/1551-5028(2000)019<1638:Domiba>2.3.Co;2

Becker, P.H., Goutner, V., Ryan, P.G., González-Solís, J., 2016. Feather mercury concentrations in Southern Ocean seabirds: Variation by species, site and time. Environ. Pollut. 216, 253–263. https://doi.org/10.1016/j.envpol.2016.05.061

Bergquist, B.A., Blum, J.D., 2007. Mass-dependent and -independent fractionation of Hg isotopes by photoreduction in aquatic systems. Science 318, 417–20. https://doi.org/10.1126/science.1148050

Blévin, P., Carravieri, A., Jaeger, A., Chastel, O., Bustamante, P., Cherel, Y., 2013. Wide range of mercury contamination in chicks of southern ocean seabirds. PLoS One 8, e54508. https://doi.org/10.1371/journal.pone.0054508

Blum, J.D., Popp, B.N., Drazen, J.C., Anela Choy, C., Johnson, M.W., 2013. Methylmercury production below the mixed layer in the North Pacific Ocean. Nat. Geosci. 6, 879–884. https://doi.org/10.1038/ngeo1918

Blum, J.D., Sherman, L.S., Johnson, M.W., 2014. Mercury isotopes in Earth and environmental sciences. Annu. Rev. Earth Planet. Sci. 42, 249–269. https://doi.org/10.1146/annurev-earth-050212-124107

Bost, C. a, Thiebot, J.B., Pinaud, D., Cherel, Y., Trathan, P.N., 2009. Where do penguins go during the inter-breeding period? Using geolocation to track the winter dispersion of the

macaroni penguin. Biol. Lett. 5, 473–476. https://doi.org/10.1098/rsbl.2009.0265

Bowman, K.L., Lamborg, C.H., Agather, A.M., 2020. A global perspective on mercury cycling in the ocean. Sci. Total Environ. 710, 136166. https://doi.org/10.1016/j.scitotenv.2019.136166

Brasso, R.L., Chiaradia, A., Polito, M.J., Raya Rey, A., Emslie, S.D., 2014. A comprehensive assessment of mercury exposure in penguin populations throughout the Southern Hemisphere: Using trophic calculations to identify sources of population-level variation. Mar. Pollut. Bull. 97, 408–418. https://doi.org/10.1016/j.marpolbul.2015.05.059

Bustamante, P., Carravieri, A., Goutte, A., Barbraud, C., Delord, K., Chastel, O., Weimerskirch, H., Cherel, Y., 2016. High feather mercury concentrations in the wandering albatross are related to sex, breeding status and trophic ecology with no demographic consequences. Environ. Res. 144, 1–10. https://doi.org/10.1016/j.envres.2015.10.024

Cai, H., Chen, J., 2015. Mass-independent fractionation of even mercury isotopes. Sci. Bull. https://doi.org/10.1007/s11434-015-0968-8

Canario, J., Santos-Echeandía, J., Koch, B.P., Laglera, L., 2017. Mercury and methylmercury in the Atlantic sector of the Southern Ocean. Deep. Res. Part II 138, 52–62. https://doi.org/10.1016/j.dsr2.2016.07.012

Carravieri, A., Bustamante, P., Churlaud, C., Cherel, Y., 2013. Penguins as bioindicators of mercury contamination in the Southern Ocean: birds from the Kerguelen Islands as a case study. Sci. Total Environ. 454–455, 141–8. https://doi.org/10.1016/j.scitotenv.2013.02.060

Carravieri, A., Bustamante, P., Labadie, P., Budzinski, H., Chastel, O., Cherel, Y., 2020. Trace elements and persistent organic pollutants in chicks of 13 seabird species from Antarctica to the subtropics. Environ. Int. 134, 105225. https://doi.org/10.1016/j.envint.2019.105225

Carravieri, A., Cherel, Y., Blévin, P., Brault-Favrou, M., Chastel, O., Bustamante, P., 2014. Mercury exposure in a large subantarctic avian community. Environ. Pollut. 190, 51–7. https://doi.org/10.1016/j.envpol.2014.03.017

Carravieri, A., Cherel, Y., Brault-Favrou, M., Churlaud, C., Peluhet, L., Labadie, P., Bustamante, P., 2017. From Antarctica to the subtropics : Contrasted geographical concentrations of selenium , mercury , and persistent organic pollutants in skua chicks (Catharacta spp .). Environ. Pollut. 228, 464–473. https://doi.org/10.1016/j.envpol.2017.05.053

Carravieri, A., Cherel, Y., Jaeger, A., Churlaud, C., Bustamante, P., 2016. Penguins as

bioindicators of mercury contamination in the southern Indian Ocean: geographical and temporal trends. Environ. Pollut. 213, 195–205. https://doi.org/10.1016/j.envpol.2016.02.010

Chandan, P., Ghosh, S., Bergquist, B.A., 2015. Mercury isotope fractionation during aqueous photoreduction of monomethylmercury in the presence of dissolved organic matter. Environ. Sci. Technol. 49, 259–267. https://doi.org/10.1021/es5034553

Chen, J., Hintelmann, H., Feng, X., Dimock, B., 2012. Unusual fractionation of both odd and even mercury isotopes in precipitation from Peterborough, ON, Canada. Geochim. Cosmochim. Acta 90, 33–46. https://doi.org/10.1016/j.gca.2012.05.005

Cherel, Y., 2008. Isotopic niches of emperor and Adélie penguins in Adélie Land, Antarctica. Mar. Biol. 154, 813–821. https://doi.org/10.1007/s00227-008-0974-3

Cherel, Y., Barbraud, C., Lahournat, M., Jaeger, A., Jaquemet, S., Wanless, R.M., Phillips, R.A., Thompson, D.R., Bustamante, P., 2018. Accumulate or eliminate? Seasonal mercury dynamics in albatrosses, the most contaminated family of birds. Environ. Pollut. 241, 124–135. https://doi.org/10.1016/j.envpol.2018.05.048

Cherel, Y., Hobson, K.A., Guinet, C., Vanpe, C., 2007. Stable isotopes document seasonal changes in trophic niches and winter foraging individual specialization in diving predators from the Southern Ocean. J. Anim. Ecol. 76, 826–836. https://doi.org/10.1111/j.1365-2656.2007.01238.x

Chouvelon, T., Spitz, J., Caurant, F., Mèndez-Fernandez, P., Autier, J., Lassus-Débat, a., Chappuis, a., Bustamante, P., 2012. Enhanced bioaccumulation of mercury in deep-sea fauna from the Bay of Biscay (north-east Atlantic) in relation to trophic positions identified by analysis of carbon and nitrogen stable isotopes. Deep. Res. Part I Oceanogr. Res. Pap. 65, 113–124. https://doi.org/10.1016/j.dsr.2012.02.010

Cossa, D., Averty, B., Pirrone, N., 2009. The origin of methylmercury in open Mediterranean waters. Limnol. Oceanogr. 54, 837–844. https://doi.org/10.4319/lo.2009.54.3.0837

Cossa, D., Heimbürger, L.-E., Lannuzel, D., Rintoul, S.R., Butler, E.C.V., Bowie, A.R., Averty, B., Watson, R.J., Remenyi, T., 2011. Mercury in the Southern Ocean. Geochim. Cosmochim. Acta 75, 4037–4052. https://doi.org/10.1016/j.gca.2011.05.001

Day, R.D., Roseneau, D.G., Berail, S., Hobson, K. a., Donard, O.F.X., Vander Pol, S.S., Pugh, R.S., Moors, A.J., Long, S.E., Becker, P.R., 2012. Mercury stable isotopes in seabird eggs reflect a gradient from terrestrial geogenic to oceanic mercury reservoirs. Environ. Sci. Technol. 46, 5327–5335. https://doi.org/10.1021/es2047156

Demers, J.D., Blum, J.D., Zak, D.R., 2013. Mercury isotopes in a forested ecosystem: Implications for air-surface exchange dynamics and the global mercury cycle. Global Biogeochem. Cycles 27, 222–238. https://doi.org/10.1002/gbc.20021

Eagles-Smith, C.A., Silbergeld, E.K., Basu, N., Bustamante, P., Diaz-Barriga, F., Hopkins, W.A., Kidd, K.A., Nyland, J.F., 2018. Modulators of mercury risk to wildlife and humans in the context of rapid global change. Ambio 47, 170–197. https://doi.org/10.1007/s13280-017-1011-x

Fitzgerald, W.F., Lamborg, C.H., Hammerschmidt, C.R., 2007. Marine biogeochemical cycling of mercury. Chem. Rev. 107, 641–62. https://doi.org/10.1021/cr050353m

Furness, R.W., Camphuysen, C.J., 1997. Seabirds as monitors of the marine environment. ICES J. Mar. Sci. 54, 726–737. https://doi.org/10.1006/jmsc.1997.0243

Gionfriddo, C.M., Tate, M.T., Wick, R.R., Schultz, M.B., Zemla, A., Thelen, M.P., Schofield, R., Krabbenhoft, D.P., Holt, K.E., Moreau, J.W., 2016. Microbial mercury methylation in Antarctic sea ice. Nat. Microbiol. 1, 16127. https://doi.org/10.1038/nmicrobiol.2016.127

Goutte, A., Barbraud, C., Meillere, A., Carravieri, A., Bustamante, P., Labadie, P., Budzinski, H., Delord, K., Cherel, Y., Weimerskirch, H., Chastel, O., 2014a. Demographic consequences of heavy metals and persistent organic pollutants in a vulnerable long-lived bird, the wandering albatross. Proc. R. Soc. B Biol. Sci. 281. https://doi.org/10.1098/rspb.2013.3313

Goutte, A., Bustamante, P., Barbraud, C., Delord, K., Weimerskirch, H., Chastel, O., 2014b. Demographic responses to mercury exposure in two closely related antarctic top predators. Ecology 95, 1075–1086. https://doi.org/10.1890/13-1229.1

Gratz, L.E., Keeler, G.J., Blum, J.D., Sherman, L.S., 2010. Isotopic composition and fractionation of mercury in Great Lakes precipitation and ambient air. Environ. Sci. Technol. 44, 7764–70. https://doi.org/10.1021/es100383w

Heimbürger, L.-E., Sonke, J.E., Cossa, D., Point, D., Lagane, C., Laffont, L., Galfond, B.T., Nicolaus, M., Rabe, B., van der Loeff, M.R., 2015. Shallow methylmercury production in the marginal sea ice zone of the central Arctic Ocean. Sci. Rep. 5, 10318. https://doi.org/10.1038/srep10318

Jiménez-Moreno, M., Perrot, V., Epov, V.N., Monperrus, M., Amouroux, D., 2013. Chemical kinetic isotope fractionation of mercury during abiotic methylation of Hg(II) by methylcobalamin in aqueous chloride media. Chem. Geol. 336, 26–36. https://doi.org/10.1016/j.chemgeo.2012.08.029

Kirk, J., St. Louis, V.L., Hintelmann, H., Lehnherr, I., Else, B., Poissant, L., 2008. Methylated Mercury Species in Marine Waters of the Canadian High and Sub Arctic. Env. Sci Technol 42, 8367–8373.

Kritee, K., Barkay, T., Blum, J.D., 2009. Mass dependent stable isotope fractionation of mercury during mer mediated microbial degradation of monomethylmercury. Geochim. Cosmochim. Acta 73, 1285–1296. https://doi.org/10.1016/j.gca.2008.11.038

Kritee, K., Blum, J.D., Barkay, T., 2008. Mercury Stable Isotope Fractionation during Reduction of Hg(II) by Different Microbial Pathways. Environ. Sci. Technol. 42, 9171–9177. https://doi.org/10.1021/es801591k

Kritee, K., Blum, J.D., Johnson, M.W., Bergquist, B.A., Barkay, T., 2007. Mercury stable isotope fractionation during reduction of Hg(II) to Hg(0) by mercury resistant microorganisms. Environ. Sci. Technol. 41, 1889–1895. https://doi.org/10.1021/es062019t

Kritee, K., Motta, L.C., Blum, J.D., Tsui, M.T.-K., Reinfelder, J.R., 2017. Photomicrobial Visible Light-Induced Magnetic Mass Independent Fractionation of Mercury in a Marine Microalga. ACS Earth Sp. Chem. acsearthspacechem.7b00056. https://doi.org/10.1021/acsearthspacechem.7b00056

Kwon, S.Y., Blum, J.D., Carvan, M.J., Basu, N., Head, J.A., Madenjian, C.P., David, S.R., 2012. Absence of fractionation of mercury isotopes during trophic transfer of methylmercury to freshwater fish in captivity. Environ. Sci. Technol. 46, 7527–34. https://doi.org/10.1021/es300794q

Lamborg, C.H., Hammerschmidt, C.R., Bowman, K.L., Swarr, G.J., Munson, K.M., Ohnemus, D.C., Lam, P.J., Heimbürger, L.-E., Rijkenberg, M.J. a., Saito, M. a., 2014. A global ocean inventory of anthropogenic mercury based on water column measurements. Nature 512, 65–68. https://doi.org/10.1038/nature13563

Lavoie, R. a, Jardine, T.D., Chumchal, M.M., Kidd, K. a, Campbell, L.M., 2013. Biomagnification of Mercury in Aquatic Food Webs: A Worldwide Meta-Analysis. Environ. Sci. Technol. 47, 13385–13394. https://doi.org/10.1021/es403103t

Lehnherr, I., St. Louis, V.L., Hintelmann, H., Kirk, J.L., 2011. Methylation of inorganic mercury in polar marine waters. Nat. Geosci. 4, 298–302. https://doi.org/10.1038/ngeo1134

Li, M., Sherman, L.S., Blum, J.D., Grandjean, P., Weihe, P., Sunderland, E.M., Shine, J.P., 2014. Assessing sources of human methylmercury exposure using stable mercury isotopes.

Environ. Sci. Technol. 48, 8800–8806.

Liu, H., Yu, B., Fu, J., Li, Y., Yang, R., Zhang, Q., Liang, Y., Yin, Y., Hu, L., Shi, J., Jiang, G., 2019. Different circulation history of mercury in aquatic biota from King George Island of the Antarctic. Environ. Pollut. 250, 892–897. https://doi.org/10.1016/j.envpol.2019.04.113

Marshall, J., Speer, K., 2012. Closure of the meridional overturning circulation through Southern Ocean upwelling. Nat. Geosci. 5, 171–180. https://doi.org/10.1038/ngeo1391

Masbou, J., Sonke, J.E., Amouroux, D., Guillou, G., Becker, P.R., Point, D., 2018. Hg-Stable Isotope Variations in Marine Top Predators of the Western Arctic Ocean. ACS Earth Sp. Chem. 0, null. https://doi.org/10.1021/acsearthspacechem.8b00017

Mason, R.P., Reinfelder, J.R., Morel, F.M.M., 1996. Uptake, toxicity and trophic transfer of Hg in a coastal diatom. Environ. Sci. Toxicol. 30, 1835–1845.

Monperrus, M., Tessier, E., Amouroux, D., Leynaert, A., Huonnic, P., Donard, O.F.X., 2007. Mercury methylation, demethylation and reduction rates in coastal and marine surface waters of the Mediterranean Sea. Mar. Chem. 107, 49–63. https://doi.org/10.1016/j.marchem.2007.01.018

Monteiro, L.R., Furness, R.W., Nevo, A.J., 1995. Mercury Levels in Seabirds from the Azores , Mid-North Atlantic Ocean 309, 304–309.

Motta, L.C., Blum, J.D., Johnson, M.W., Umhau, B.P., Popp, B.N., Washburn, S.J., Drazen, J.C., Benitez-Nelson, C.R., Hannides, C.C.S., Close, H.G., Lamborg, C.H., 2019. Mercury Cycling in the North Pacific Subtropical Gyre as Revealed by Mercury Stable Isotope Ratios. Global Biogeochem. Cycles 33, 777–794. https://doi.org/10.1029/2018GB006057

Perrot, V., Bridou, R., Pedrero, Z., Guyoneaud, R., Monperrus, M., Amouroux, D., 2015. Identical Hg isotope mass dependent fractionation signature during methylation by sulfate-reducing bacteria in sulfate and sulfate-free environment. Environ. Sci. Technol. 49, 1365–1373. https://doi.org/10.1021/es5033376

Perrot, V., Pastukhov, M. V, Epov, V.N., Husted, S., Donard, O.F.X., Amouroux, D., 2012. Higher mass-independent isotope fractionation of methylmercury in the pelagic food web of Lake Baikal (Russia). Environ. Sci. Technol. 46, 5902–11. https://doi.org/10.1021/es204572g

Pickhardt, P.C., Folt, C.L., Chen, C.Y., Klaue, B., Blum, J.D., 2002. Algal blooms reduce the uptake of toxic methylmercury in freshwater food webs. Proc. Natl. Acad. Sci. U. S. A. 99, 4419–23. https://doi.org/10.1073/pnas.072531099

Point, D., Sonke, J.E., Day, R.D., Roseneau, D.G., Hobson, K.A., Pol, S.S. Vander, Moors, A.J., Pugh, R.S., Donard, O.F.X., Becker, P.R., 2011. Methylmercury photodegradation influenced by sea-ice cover in Arctic marine ecosystems. Nat. Geosci. 4, 1–7. https://doi.org/10.1038/ngeo1049

Queipo Abad, S., Rodríguez-González, P., Davis, W.C., García Alonso, J.I., 2017. Development of a Common Procedure for the Determination of Methylmercury, Ethylmercury, and Inorganic Mercury in Human Whole Blood, Hair, and Urine by Triple Spike Species-Specific Isotope Dilution Mass Spectrometry. Anal. Chem. 89, 6731–6739. https://doi.org/10.1021/acs.analchem.7b00966

Renedo, M., Amouroux, D., Cherel, Y., Bustamante, P., 2018a. Identification of sources and bioaccumulation pathways of MeHg in subantarctic penguins : a stable isotopic investigation. Sci. Rep. 1–10. https://doi.org/10.1038/s41598-018-27079-9

Renedo, M., Amouroux, D., Duval, B., Carravieri, A., Tessier, E., Barre, J., Bérail, S., Pedrero, Z., Cherel, Y., Bustamante, P., 2018b. Seabird Tissues As Efficient Biomonitoring Tools for Hg Isotopic Investigations: Implications of Using Blood and Feathers from Chicks and Adults. Environ. Sci. Technol. 52, 4227–4234. https://doi.org/10.1021/acs.est.8b00422

Riaux-Gobin, C., Dieckmann, G.S., Poulin, M., Neveux, J., Labrune, C., Vétion, G., 2013. Environmental conditions, particle flux and sympagic microalgal succession in spring before the sea-ice break-up in Adélie Land, East Antarctica. Polar Res. 32. https://doi.org/10.3402/polar.v32i0.19675

Rodrigues, J.L., Rodriguez Alvarez, C., Rodriguez Farinas, N., Berzas Nevado, J.J., Barbosa, F.J., Rodriguez Martin-Doimeadios, R.C., 2011. Mercury speciation in whole blood by gas chromatography coupled to ICP-MS with a fast microwave-assisted sample preparation procedure. J. Anal. At. Spectrom. 26, 436–442. https://doi.org/10.1039/c004931j

Rodriguez Gonzalez, P., Epov, V.N., Bridou, R., Tessier, E., Guyoneaud, R., Monperrus, M., Amouroux, D., 2009. Species-specific stable isotope fractionation of mercury during Hg (II) methylation by an anaerobic bacteria (Desulfobulbus propionicus) under dark conditions. Environ. Sci. Technol. 43, 9183–9188.

Rose, C.H., Ghosh, S., Blum, J.D., Bergquist, B.A., 2015. Effects of ultraviolet radiation on mercury isotope fractionation during photo-reduction for inorganic and organic mercury species. Chem. Geol. 405, 102–111. https://doi.org/10.1016/j.chemgeo.2015.02.025

Sallée, J.B., Speer, K.G., Rintoul, S.R., 2010. Zonally asymmetric response of the Southern

Ocean mixed-layer depth to the Southern. Nat. Geosci. 3, 273–279. https://doi.org/10.1038/ngeo812

Senn, D.B., Chesney, E.J., Blum, J.D., Bank, M.S., Maage, A., Shine, J.P., 2010. Study of Methylmercury Sources and Trophic Transfer in the Northern Gulf of Mexico. Environ. Sci. Technol. 44, 1630−1637.

Sherman, L.S., Blum, J.D., Douglas, T.A., Steffen, A., 2012a. Frost flowers growing in the Arctic ocean-atmosphere-sea ice-snow interface: 2. Mercury exchange between the atmosphere, snow, and frost flowers. J. Geophys. Res. Atmos. 117, 1–10. https://doi.org/10.1029/2011JD016186

Sherman, L.S., Blum, J.D., Johnson, K.P., Keeler, G.J., Barres, J. a., Douglas, T. a., 2010. Mass-independent fractionation of mercury isotopes in Arctic snow driven by sunlight. Nat. Geosci. 3, 173–177. https://doi.org/10.1038/ngeo758

Sherman, L.S., Blum, J.D., Keeler, G.J., Demers, J.D., Dvonch, J.T., 2012b. Investigation of local mercury deposition from a coal-fired power plant using mercury isotopes. Environ. Sci. Technol. 46, 382–390. https://doi.org/10.1021/es202793c

Soerensen, A.L., Jacob, D.J., Schartup, A.T., Fisher, J.A., Lehnherr, I., Louis, V.L.S., Heimbürger, L., Sonke, J.E., Krabbenhoft, D.P., Sunderland, E.M., 2016. Global Biogeochemical Cycles in the Arctic Ocean. Global Biogeochem. Cycles 560–575. https://doi.org/10.1002/2015GB005280.Received

Sokolov, S., 2008. Chlorophyll blooms in the Antarctic Zone south of Australia and New Zealand in reference to the Antarctic Circumpolar Current fronts and sea ice forcing. J. Geophys. Res. Ocean. 113. https://doi.org/10.1029/2007JC004329

Sokolov, S., Rintoul, S.R., 2007. On the relationship between fronts of the Antarctic Circumpolar Current and surface chlorophyll concentrations in the Southern Ocean. J. Geophys. Res. Ocean. 112, 1–17. https://doi.org/10.1029/2006JC004072

Sullivan, C.W., Arrigo, K.R., Mcclain, C.R., Comiso, J.C., Firestone, J., 1993. Distributions of phytoplankton blooms in the Southern Ocean. Science (80-.). 262, 1832–1837.

Sunderland, E.M., Krabbenhoft, D.P., Moreau, J.W., Strode, S.A., Landing, W.M., 2009. Mercury sources, distribution, and bioavailability in the North Pacific Ocean: Insights from data and models. Global Biogeochem. Cycles 23, 1–14. https://doi.org/10.1029/2008GB003425

Tartu, S., Goutte, A., Bustamante, P., Angelier, F., Moe, B., Clément-Chastel, C., Bech, C., Gabrielsen, G.W., Bustnes, J.O., Chastel, O., 2013. To breed or not to breed: endocrine

response to mercury contamination by an Arctic seabird. Biol. Lett. 9, 20130317. https://doi.org/10.1098/rsbl.2013.0317

Tripathy, S.C., Pavithran, S., Sabu, P., Pillai, H.U.K., Dessai, D.R.G., Anilkumar, N., 2015. Deep-Sea Research II Deep chlorophyll maximum and primary productivity in Indian Ocean sector of the Southern Ocean : Case study in the Subtropical and Polar Front during austral summer 2011. Deep. Res. Part II 118, 240–249. https://doi.org/10.1016/j.dsr2.2015.01.004

Watras, C.J., Back, R.C., Halvorsen, S., Hudson, R.J.M., Morrison, K.A., Wente, S.P., 1998. Bioaccumulation of mercury in pelagic freshwater food webs. Sci. Total Environ. 219, 183–208. https://doi.org/10.1016/S0048-9697(98)00228-9

Yamakawa, A., Takeuchi, A., Shibata, Y., Berail, S., Donard, O.F.X., 2016. Determination of Hg isotopic compositions in certified reference material NIES No. 13 Human Hair by cold vapor generation multi-collector inductively coupled plasma mass spectrometry. Accredit. Qual. Assur.

Zheng, W., Hintelmann, H., 2010. Isotope fractionation of mercury during its photochemical reduction by low-molecular-weight organic compounds. J. Phys. Chem. A 114, 4246–4253.

Zheng, W., Hintelmann, H., 2009. Mercury isotope fractionation during photoreduction in natural water is controlled by its Hg/DOC ratio. Geochim. Cosmochim. Acta 73, 6704–6715. https://doi.org/10.1016/j.gca.2009.08.016

Zheng, W., Xie, Z., Bergquist, B.A., 2015. Mercury stable isotopes in ornithogenic deposits as tracers of historical cycling of mercury in Ross Sea, Antarctica. Env. Sci Technol 49, 7623–7632. https://doi.org/10.1021/acs.est.5b00523

Supporting Information

A “seabird-eye” on mercury stable isotopes and cycling in the Southern Ocean

Marina Renedo[a,b,*], Paco Bustamante[a,c], Yves Cherel[d], Zoyne Pedrero[b], Emmanuel Tessier[b], David Amouroux[b,*]

[a] Littoral Environnement et Sociétés (LIENSs), UMR 7266 CNRS- La Rochelle Université, 2 rue Olympe de Gouges, 17000 La Rochelle, France

[b] Universite de Pau et des Pays de l’Adour, E2S UPPA, CNRS, IPREM, Institut des Sciences Analytiques et de Physico-chimie pour l’Environnement et les matériaux, Pau, France

[c] Institut Universitaire de France (IUF), 1 rue Descartes 75005 Paris, France

[d] Centre d'Etudes Biologiques de Chizé (CEBC), UMR 7372 CNRS-La Rochelle Université, 79360 Villiers-en-Bois, France

**Corresponding authors:* marina.renedo@ird.fr, david.amouroux@univ-pau.fr

Table of content

Section 1. Supplemental figures and tables

Experimental

Hg isotopic composition analyses

Hg isotopic compositions of samples are reported using delta notation according to the following equations:

$$\delta^{xxx}\,Hg = [(^{xxx/198}Hg_{sample} / {}^{xxx/198}Hg_{\,NIST\ 3133}) - 1)] \cdot 1000\ (‰) \qquad (1)$$

MIF signatures are expressed using capital delta notation, as suggested elsewhere (Bergquist and Blum, 2007), according to the following equations:

$$\Delta^{204}Hg = \delta^{204}Hg - (1.493 \cdot \delta^{202}Hg) \qquad (2)$$

$$\Delta^{201}Hg = \delta^{201}Hg - (0.752 \cdot \delta^{202}Hg) \qquad (3)$$

$$\Delta^{200}Hg = \delta^{200}Hg - (0.502 \cdot \delta^{202}Hg) \qquad (4)$$

$$\Delta^{199}Hg = \delta^{199}Hg - (0.252 \cdot \delta^{202}Hg) \qquad (5)$$

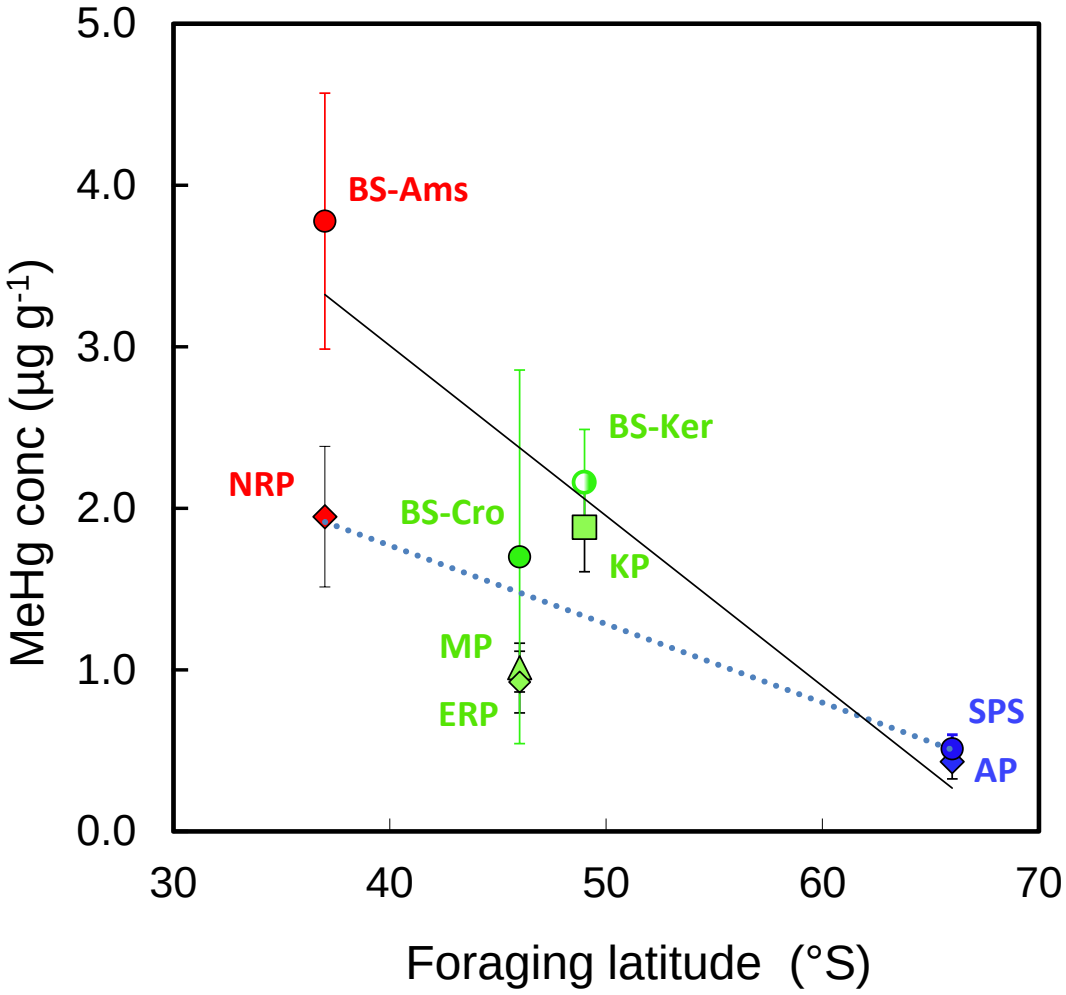

Figure S1. Mean MeHg concentrations (dry weight, µg g^{-1}) versus foraging latitude for blood samples of skua chicks and penguin adults from the Southern Ocean. Regression equations for skua MeHg concentration blood-latitude (y= -0.10x+7.22, Adj. R^2=0.62, p<0.0001) and for penguin MeHg blood-latitude (y= -0.05x+3.71, Adj. R^2=0.33, p<0.0001).

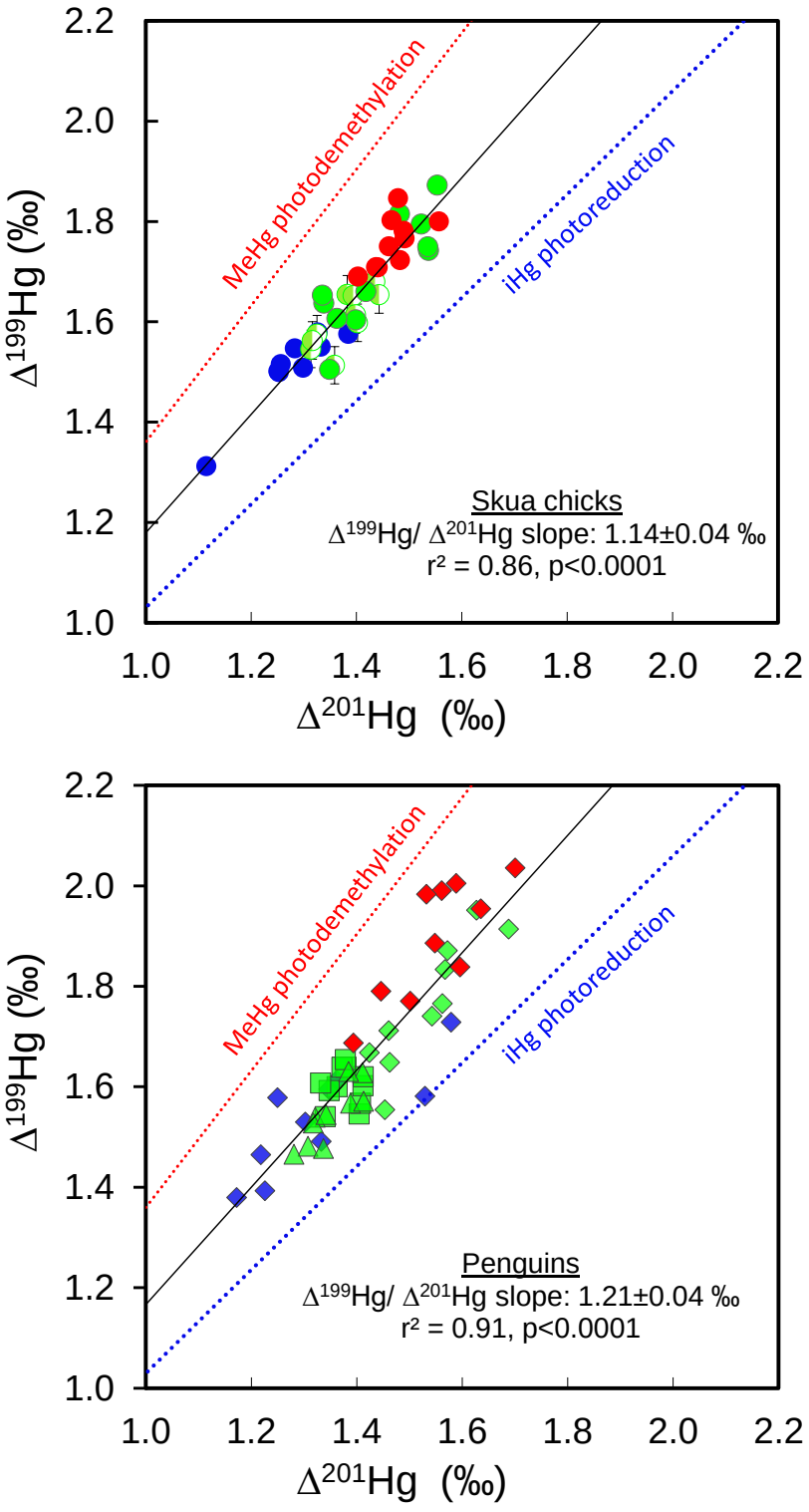

Figure S2. Hg odd-MIF signatures (Δ^{199}Hg versus Δ^{201}Hg) for blood samples of skua chicks (A) and penguins (B) from the Southern Ocean. See Figure 1 for legend. The solid line represents the Δ^{199}Hg/Δ^{201}Hg slope of the samples. The red dashed line represents the theoretical Δ^{199}Hg/Δ^{201}Hg slope for MeHg photodemethylation in the water column and the blue dashed line represents the theoretical Δ^{199}Hg/Δ^{201}Hg slope expected for photoreduction of Hg(II) in the water column (Bergquist and Blum, 2007).

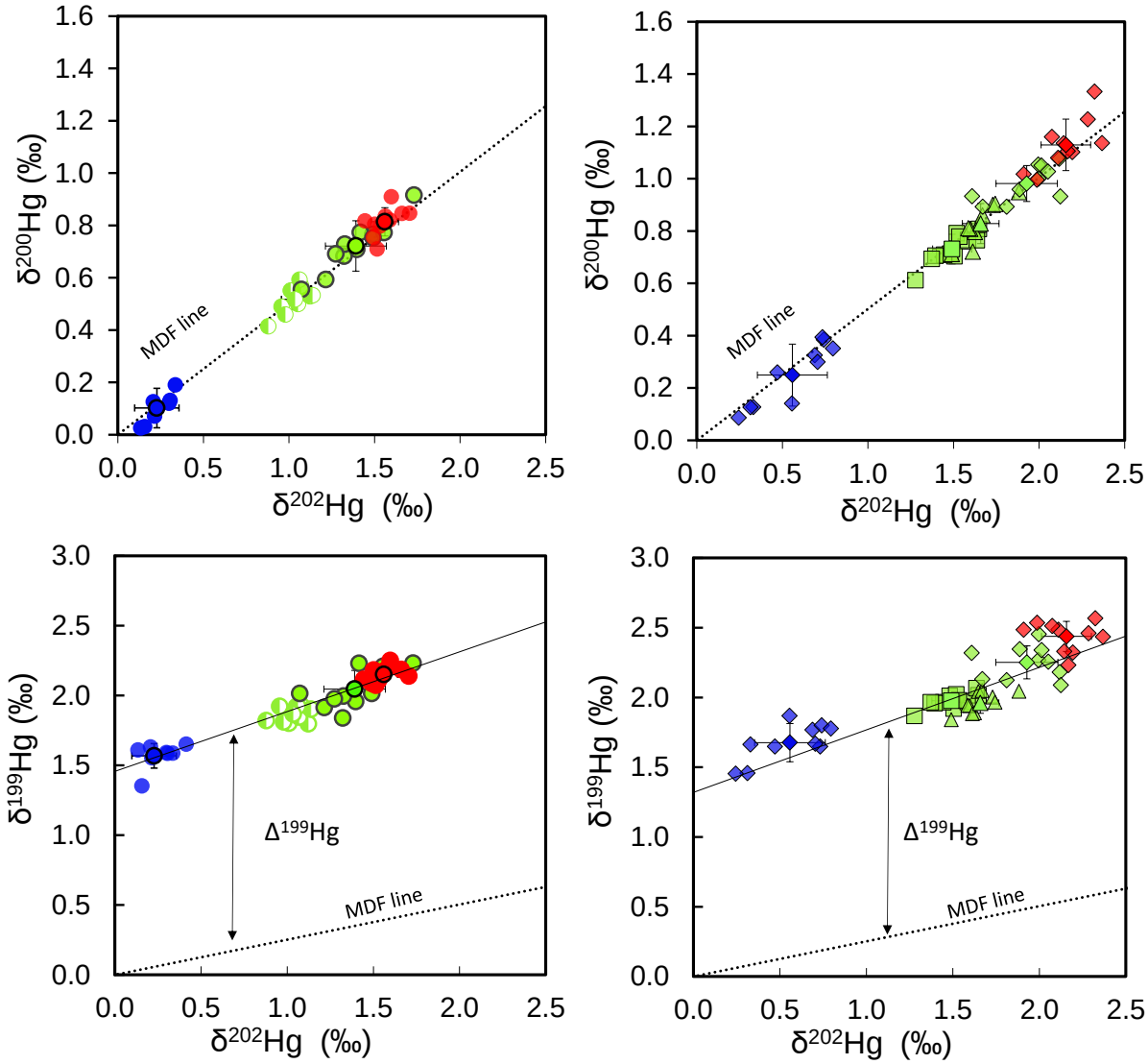

Figure S3. Hg MDF and odd-MIF signatures for blood of skua chicks (left side) and of penguins (right side) from the Southern Ocean. A) δ^{202}Hg versus δ^{200}Hg, B) δ^{202}Hg versus δ^{199}Hg. Blue (Adélie Land), green (Crozet and Kerguelen) and red (Amsterdam). The dotted lines represent the theoretically predicted MDF based on δ^{202}Hg.

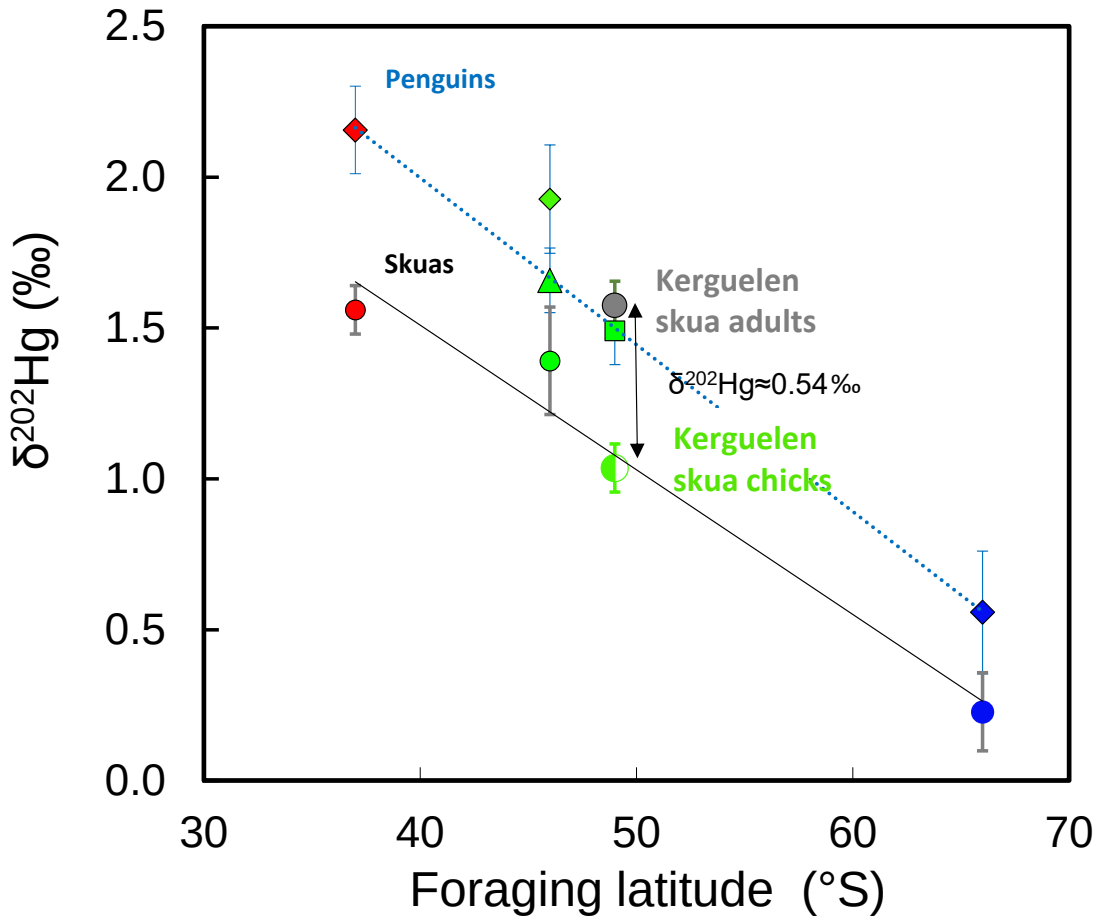

Figure S4. Hg MDF results showing δ^{202}Hg differences between adult and chicks of the Kerguelen community.

Table S1. Mean values of Hg concentrations and Hg speciation obtained for reference materials with validated THg and MeHg concentration values: ERM-CE-464 (tuna fish), Dolt-4 (dogfish liver); and internal reference materials: RBC-KP (penguin red blood cells). Values are Mean±SD.

Tissue	Reference material			Concentrations ($ng \cdot g^{-1}$)			Recoveries (%)	
			n	MeHg	iHg	THg	MeHg (%)	THg(%)
Human hair (CRM)	NIES-13	**Certified values**		**3800±400**		**4420±200**		
		This study	3	3647±46		4238±52	96±1	96±1
Tuna fish (CRM)	ERM-CE-464	**Certified values**		**5117±158**		**5240±100**		
		This study	3	4809±61	265±11	5074±67	94±1	97±1
Dogfish liver (CRM)	Dolt-4	**Certified values**		**1330±120**		**2580±220**		
		This study	3	1202±13	1154±42	2516±81	95 ±3	98 ±3
Penguin red blood cells (IRM)	RBC-KP	**Values AMA-254**				**1980±76**		
		This study	3	1956±38	62±13	1988±39		101±2

Table S2. Mean values of Hg isotopic composition obtained for reference materials with validated reference isotopic values: NIST RM 8610 (former UM-Almadén), NIST SRM 1947 (Lake Michigan fish tissue) and NIES-13 (human hair); previously published intercomparison values: IAEA-086 (human hair), ERM-CE-464 (tuna fish); and internal reference materials: F-KP (penguin feathers) and RBC-KP (penguin red blood cells). Values are Mean±SD.

Sample	Reference	n	δ^{204}Hg±2SD ‰	δ^{202}Hg±2SD ‰	δ^{201}Hg±2SD ‰	δ^{200}Hg±2SD ‰	δ^{199}Hg±2SD ‰	Δ^{204}Hg±2SD ‰	Δ^{201}Hg±2SD ‰	Δ^{200}Hg±2SD ‰	Δ^{199}Hg±2SD ‰
NIST RM 8610 (UM Almadén)	This study	77	-0.84±0.22	-0.55±0.16	-0.45±0.13	-0.27±0.51	-0.17±0.12	-0.01±0.16	-0.04±0.09	0.00±0.11	-0.03±0.11
	Reference values		-0.82±0.07	-0.56±0.03	-0.46±0.02	-0.27±0.01	-0.17±0.01	-	-0.04±0.01	0.00±0.01	-0.03±0.02
NIST SRM 1947	This study	4	1.68±0.25	1.19±0.10	5.02±0.15	0.69±0.09	5.54±0.14	-0.09±0.12	4.13±0.12	0.09±0.05	5.25±0.13
	Reference values		1.66±0.07	1.20±0.07	5.09±0.18	0.69±0.09	5.62±0.25	-0.13±0.02	4.17±0.28	0.09±0.02	5.31±0.29
NIES-13	This study	8	2.99±0.22	2.08±0.15	3.07±0.16	1.09±0.10	2.34±0.10	-0.12±0.28	1.51±0.06	0.04±0.04	1.81±0.09
	Yamakawa et al., 2016	11	2.76±0.16	1.89±0.10	2.77±0.10	0.98±0.08	2.13±0.07	-0.04±0.11	1.36±0.07	0.04±0.04	1.65±0.06
IAEA-086	This study	6	0.94±0.25	0.73±0.13	0.77±0.09	0.37±0.11	0.44±0.16	-0.14±0.26	0.22±0.08	0.00±0.09	0.26±0.15

	Yamakawa et al., 2016	3	0.87±0.12	0.58±0.09	0.64±0.09	0.31±0.04	0.41±0.02	0.00±0.04	0.20±0.03	0.02±0.04	0.26±0.02
ERM-CE-464	This study	2	0.91±0.13	0.64±0.04	2.37±0.03	0.40±0.01	2.49±0.01	-0.04±0.19	1.89±0.05	0.08±0.01	2.33±0.01
	Li et al., 2014	9	0.94±0.06	0.70±0.04	2.49	0.43±0.05	2.55±0.08	-	1.96±0.06	0.07±0.04	2.38±0.07
F-KP	This study	17	2.40±0.25	1.58±0.22	2.67±0.21	0.80±0.16	2.11±0.18	0.04±0.24	1.48±0.13	0.01±0.09	1.71±0.15
RBC-KP	This study	7	1.98±0.18	1.30±0.13	2.26±0.14	0.64±0.13	1.78±0.17	0.04±0.10	1.28±0.09	-0.01±0.09	1.46±0.14

Table S3. Total and MeHg concentrations (µg g^{-1}), Hg isotopic composition (‰) and carbon ($\delta^{13}C$, ‰) and nitrogen ($\delta^{15}N$, ‰) isotopes for all the skua individuals from the four studied populations from the Southern Ocean.

Species	Location	Latitude	Sampling	Code	MeHg (µg g^{-1})	THg (µg g^{-1})	$\delta^{204}Hg$ (‰)	$\delta^{202}Hg$ (‰)	$\delta^{201}Hg$ (‰)	$\delta^{200}Hg$ (‰)	$\delta^{199}Hg$ (‰)	$\Delta^{204}Hg$ (‰)	$\Delta^{201}Hg$ (‰)	$\Delta^{200}Hg$ (‰)	$\Delta^{199}Hg$ (‰)	$\delta^{13}C$ (‰)	$\delta^{15}N$ (‰)
South polar skua	Adélie Land	66°40'S	Dec-Jan 2012	ASP 01	0.56	0.59	0.55	0.31	1.53	0.13	1.59	0.09	1.30	-0.02	1.51	-23.39	11.48
South polar skua	Adélie Land	66°40'S	Dec-Jan 2012	ASP 02	0.55	0.61	0.08	-0.02	1.32	0.00	1.55	0.11	1.33	0.01	1.55	-23.58	11.32
South polar skua	Adélie Land	66°40'S	Dec-Jan 2012	ASP 03	0.56	0.59	0.19	0.22	1.41	0.07	1.55	-0.13	1.25	-0.04	1.50	-23.38	11.56
South polar skua	Adélie Land	66°40'S	Dec-Jan 2012	ASP 04	0.39	0.44	0.23	0.13	1.49	0.03	1.61	0.03	1.38	-0.04	1.58	-23.54	11.55
South polar skua	Adélie Land	66°40'S	Dec-Jan 2012	ASP 05	0.38	0.43	0.50	0.34	1.51	0.19	1.59	0.00	1.25	0.02	1.50	-23.02	10.03
South polar skua	Adélie Land	66°40'S	Dec-Jan 2012	ASP 08	0.40	0.50	0.29	0.16	1.23	0.03	1.35	0.05	1.12	-0.05	1.31	-23.73	11.76
South polar skua	Adélie Land	66°40'S	Dec-Jan 2012	ASP 09	0.40	0.45	0.36	0.21	1.48	0.13	1.63	0.05	1.33	0.02	1.58	-23.66	11.61
South polar skua	Adélie Land	66°40'S	Dec-Jan 2012	ASP 10	0.49	0.55	0.45	0.30	1.48	0.12	1.59	0.01	1.26	-0.03	1.52	-23.74	11.52
South polar skua	Adélie Land	66°40'S	Dec-Jan 2012	ASP 11	0.59	0.65	0.53	0.41	1.60	0.22	1.65	-0.09	1.28	0.01	1.55	-23.34	11.35
Brown skua	Kerguelen	49°21′S	Dec 2011	SSKERP01	2.37	2.48	1.54	1.08	2.20	0.54	1.93	-0.08	1.38	-0.01	1.65	-22.51	10.30
Brown skua	Kerguelen	49°21′S	Dec 2011	SSKERP02	1.83	1.94	1.64	1.05	2.19	0.50	1.92	0.06	1.39	-0.03	1.65	-22.68	10.20

Brown skua	Kerguelen	49°21′S	Dec 2011	SSKER P03	2.03	2.14	1.46	0.96	2.16	0.49	1.92	0.03	1.44	0.01	1.68	-22.76	10.13
Brown skua	Kerguelen	49°21′S	Dec 2011	SSKER P04	1.78	2.03	1.36	0.88	2.06	0.41	1.82	0.05	1.40	-0.03	1.60	-22.84	10.29
Brown skua	Kerguelen	49°21′S	Dec 2011	SSKER P05	2.50	2.69	1.60	1.12	2.20	0.53	1.80	-0.07	1.36	-0.04	1.51	-22.84	10.13
Brown skua	Kerguelen	49°21′S	Dec 2011	SSKER P06	2.22	2.37	1.60	1.01	2.07	0.55	1.80	0.09	1.31	0.04	1.55	-22.60	10.34
Brown skua	Kerguelen	49°21′S	Dec 2011	SSKER P07	1.64	1.77	1.55	1.07	2.13	0.57	1.85	-0.05	1.33	0.03	1.58	-22.55	10.36
Brown skua	Kerguelen	49°21′S	Dec 2011	SSKER P08	2.30	2.47	1.45	0.98	2.05	0.46	1.81	-0.02	1.32	-0.03	1.56	-23.19	9.99
Brown skua	Kerguelen	49°21′S	Dec 2011	SSKER P09	2.62	2.83	1.74	1.14	2.25	0.53	1.90	0.04	1.40	-0.04	1.61	-22.49	10.58
Brown skua	Kerguelen	49°21′S	Dec 2011	SSKER P10	2.32	2.51	1.53	1.06	2.24	0.59	1.92	-0.06	1.44	0.06	1.65	-22.98	10.18
Brown skua adult	Kerguelen	49°21′S	Dec 2011	SSKER A01	10.73	11.87	2.48	1.64	2.48	0.82	1.90	0.04	1.25	0.00	1.49	-21.75	11.24
Brown skua adult	Kerguelen	49°21′S	Dec 2011	SSKER A02	7.51	8.52	2.32	1.53	2.45	0.74	1.86	0.03	1.29	-0.03	1.47	-20.97	11.25
Brown skua adult	Kerguelen	49°21′S	Dec 2011	SSKER A03	9.69	10.55	2.17	1.42	2.38	0.68	1.83	0.06	1.32	-0.03	1.48	-21.31	11.25
Brown skua adult	Kerguelen	49°21′S	Dec 2011	SSKER A04	10.60	11.22	2.32	1.55	2.50	0.77	1.91	0.00	1.33	-0.01	1.52	-21.64	11.20
Brown skua adult	Kerguelen	49°21′S	Dec 2011	SSKER A05	14.36	15.16	2.52	1.66	2.54	0.83	1.93	0.04	1.29	-0.01	1.51	-21.49	11.25

Brown skua adult	Kergue len	49°21′S	Dec 2011	SSKER A06	10.75	11.32	2.41	1.59	2.53	0.78	1.86	0.04	1.34	-0.02	1.46	-21.70	11.25
Brown skua adult	Kergue len	49°21′S	Dec 2011	SSKER A07	8.70	9.24	2.43	1.63	2.52	0.83	1.95	0.00	1.30	0.02	1.54	-21.27	11.25
Brown skua adult	Kergue len	49°21′S	Dec 2011	SSKER A08	11.57	12.32	2.65	1.65	2.48	0.80	1.89	0.18	1.24	-0.03	1.48	-21.55	11.32
Brown skua adult	Kergue len	49°21′S	Dec 2011	SSKER A10	8.64	9.25	2.25	1.51	2.44	0.84	1.92	-0.01	1.30	0.08	1.54	-21.82	11.17
Brown skua	Crozet	46°26′S	Jan-Feb 2012	SSCR OP01	2.10	2.43	2.14	1.40	2.45	0.71	1.96	0.05	1.40	0.01	1.60	-20.62	11.39
Brown skua	Crozet	46°26′S	Jan-Feb 2012	SSCR OP02	2.91	2.96	2.02	1.32	2.34	0.68	1.84	0.04	1.35	0.02	1.51	-20.57	11.44
Brown skua	Crozet	46°26′S	Jan-Feb 2012	SSCR OP03	1.07	1.14	1.86	1.33	2.42	0.73	2.00	-0.12	1.42	0.06	1.66	-19.59	10.58
Brown skua	Crozet	46°26′S	Jan-Feb 2012	SSCR OP04	4.38	4.52	2.20	1.49	2.46	0.76	2.01	-0.03	1.34	0.02	1.64	-20.56	11.27
Brown skua	Crozet	46°26′S	Jan-Feb 2012	SSCR OP05	2.50	2.68	1.93	1.22	2.28	0.59	1.91	0.11	1.36	-0.02	1.61	-20.28	11.05
Brown skua	Crozet	46°26′S	Jan-Feb 2012	SSCR OP06	0.67	0.74	2.19	1.56	2.65	0.77	2.21	-0.13	1.48	-0.01	1.82	-19.91	10.65
Brown skua	Crozet	46°26′S	Jan-Feb 2012	SSCR OP07	1.09	1.18	2.54	1.73	2.83	0.92	2.23	-0.04	1.52	0.05	1.79	-19.64	10.20
Brown skua	Crozet	46°26′S	Jan-Feb 2012	SSCR OP08	0.88	0.93	1.64	1.07	2.34	0.55	2.01	0.04	1.54	0.02	1.74	-20.91	9.76
Brown skua	Crozet	46°26′S	Jan-Feb 2012	SSCR OP09	1.17	1.25	2.02	1.42	2.62	0.77	2.23	-0.10	1.55	0.06	1.87	-20.15	10.57

Brown skua	Crozet	46°26′S	Jan-Feb 2012	SSCR OP10	0.89	0.93	1.92	1.27	2.29	0.69	1.97	0.02	1.34	0.05	1.65	-20.26	9.64
Brown skua	Crozet	46°26′S	Jan-Feb 2012	SSCR OP11	1.02	1.09	2.26	1.49	2.66	0.75	2.13	0.03	1.54	0.00	1.75	-20.27	9.65
Brown skua	Amster dam	37°50′S	Dec 2011	SSAM S12P01	3.30	3.34	2.21	1.50	2.60	0.80	2.18	-0.03	1.47	0.05	1.80	-17.82	14.55
Brown skua	Amster dam	37°50′S	Dec 2011	SSAM S12P02	4.27	4.33	2.32	1.56	2.67	0.83	2.18	-0.01	1.49	0.05	1.78	-17.71	14.34
Brown skua	Amster dam	37°50′S	Dec 2011	SSAM S12P03	3.96	4.51	2.26	1.44	2.55	0.82	2.11	0.10	1.46	0.09	1.75	-17.53	14.42
Brown skua	Amster dam	37°50′S	Dec 2011	SSAM S12P04	3.28	3.44	2.33	1.60	2.68	0.91	2.25	-0.05	1.48	0.11	1.85	-17.56	14.32
Brown skua	Amster dam	37°50′S	Dec 2011	SSAM S12P05	4.47	4.94	2.18	1.52	2.54	0.71	2.07	-0.08	1.40	-0.05	1.69	-17.63	14.11
Brown skua	Amster dam	37°50′S	Dec 2011	SSAM S12P06	5.54	5.82	2.40	1.71	2.72	0.85	2.14	-0.15	1.44	-0.01	1.71	-18.30	14.81
Brown skua	Amster dam	37°50′S	Dec 2011	SSAM S12P07	2.93	3.00	2.39	1.66	2.74	0.85	2.18	-0.09	1.49	0.01	1.77	-16.89	14.42
Brown skua	Amster dam	37°50′S	Dec 2011	SSAM S12P08	3.47	3.81	2.21	1.49	2.56	0.75	2.09	-0.02	1.44	0.00	1.71	-17.98	14.12
Brown skua	Amster dam	37°50′S	Dec 2011	SSAM S12P09	3.31	3.43	2.48	1.59	2.75	0.82	2.20	0.11	1.56	0.02	1.80	-17.54	14.28
Brown skua	Amster dam	37°50′S	Dec 2011	SSAM S12P10	3.24	3.38	2.30	1.53	2.63	0.80	2.11	0.01	1.48	0.03	1.72	-17.69	14.30

Table S4. Total and MeHg concentrations (µg g^{-1}), Hg isotopic composition (‰) and carbon ($\delta^{13}C$, ‰) and nitrogen ($\delta^{15}N$, ‰) isotopes for all the penguin individuals from the five studied populations from the Southern Ocean.

Species	Location	Latitude	Sampling date	Code	MeHg (µg g^{-1})	THg (µg g^{-1})	$\delta^{204}Hg$ (‰)	$\delta^{202}Hg$ (‰)	$\delta^{201}Hg$ (‰)	$\delta^{200}Hg$ (‰)	$\delta^{199}Hg$ (‰)	$\Delta^{204}Hg$ (‰)	$\Delta^{201}Hg$ (‰)	$\Delta^{200}Hg$ (‰)	$\Delta^{199}Hg$ (‰)	$\delta^{13}C$ (‰)	$\delta^{15}N$ (‰)
Adélie penguin	Adélie Land	66°40'S	Feb 2012	APA11	0.42	0.45	1.03	0.69	1.87	0.33	1.77	0.00	1.35	-0.02	1.60	-24.01	8.88
Adélie penguin	Adélie Land	66°40'S	Feb 2012	APA12	0.38	0.42	0.52	0.33	1.78	0.13	1.66	0.03	1.53	-0.04	1.58	-24.35	8.99
Adélie penguin	Adélie Land	66°40'S	Feb 2012	APA13	0.48	0.50	1.14	0.74	1.92	0.38	1.80	0.03	1.36	0.01	1.61	-24.28	9.22
Adélie penguin	Adélie Land	66°40'S	Feb 2012	APA14	0.38	0.40	0.45	0.31	1.41	0.13	1.46	-0.01	1.17	-0.03	1.38	-24.17	9.45
Adélie penguin	Adélie Land	66°40'S	Feb 2012	APA15	0.48	0.64	1.02	0.73	1.77	0.39	1.65	-0.07	1.22	0.03	1.47	-24.02	10.12
Adélie penguin	Adélie Land	66°40'S	Feb 2012	APA16	0.46	0.49	1.09	0.79	1.85	0.35	1.78	-0.10	1.25	-0.05	1.58	-24.23	9.67
Adélie penguin	Adélie Land	66°40'S	Feb 2012	APA17	0.18	0.18	0.71	0.56	2.00	0.14	1.87	-0.12	1.58	-0.14	1.73	-24.17	8.48
Adélie penguin	Adélie Land	66°40'S	Feb 2012	APA18	0.56	0.58	0.77	0.47	1.66	0.26	1.65	0.07	1.30	0.02	1.53	-24.16	10.04
Adélie penguin	Adélie Land	66°40'S	Feb 2012	APA19	0.52	0.55	1.10	0.71	1.86	0.30	1.67	0.04	1.33	-0.06	1.49	-24.04	9.63
Adélie penguin	Adélie Land	66°40'S	Feb 2012	APA20	0.45	0.45	0.37	0.24	1.41	0.09	1.45	0.01	1.23	-0.04	1.39	-24.23	9.71

Emperor penguin chick	Adélie Land	66°40’S	Nov 2011	EPP 01	0.55	1.43	0.78	0.55	1.43	0.25	1.34	-0.04	1.01	-0.02	1.20	-25.56	12.51
Emperor penguin chick	Adélie Land	66°40’S	Nov 2011	EPP 02	0.57	1.37	0.76	0.57	1.37	0.15	1.15	-0.09	0.94	-0.13	1.01	-25.85	12.75
Emperor penguin chick	Adélie Land	66°40’S	Nov 2011	EPP 03	0.38	1.20	0.50	0.38	1.20	0.10	1.06	-0.07	0.91	-0.10	0.96	-25.80	12.75
Emperor penguin chick	Adélie Land	66°40’S	Nov 2011	EPP 04	0.59	1.37	0.74	0.59	1.37	0.18	1.20	-0.14	0.93	-0.12	1.05	-25.79	12.84
Emperor penguin chick	Adélie Land	66°40’S	Nov 2011	EPP 05	0.48	1.36	0.72	0.48	1.36	0.20	1.28	0.00	1.00	-0.04	1.16	-25.64	12.58
Emperor penguin chick	Adélie Land	66°40’S	Nov 2011	EPP 06	0.57	1.43	1.01	0.57	1.43	0.31	1.36	0.15	1.00	0.02	1.21	-26.02	12.74
Emperor penguin chick	Adélie Land	66°40’S	Nov 2011	EPP 07	0.48	1.30	0.70	0.48	1.30	0.16	1.29	-0.02	0.94	-0.09	1.17	-25.25	12.55
Emperor penguin chick	Adélie Land	66°40’S	Nov 2011	EPP 08	0.72	1.58	1.20	0.72	1.58	0.50	1.51	0.12	1.04	0.13	1.33	-25.87	12.60
Emperor penguin chick	Adélie Land	66°40’S	Nov 2011	EPP 09	0.51	1.39	0.78	0.51	1.39	0.20	1.29	0.03	1.01	-0.06	1.16	-25.67	13.03
Emperor penguin chick	Adélie Land	66°40’S	Nov 2011	EPP 10	0.48	1.33	0.69	0.48	1.33	0.16	1.15	-0.03	0.97	-0.08	1.03	-25.85	12.83

King penguin	Crozet	46°26′S	Oct 2011	KPA01	1.71	1.85	2.51	1.65	2.60	0.81	2.02	0.05	1.36	-0.02	1.60	-21.76	10.10
King penguin	Crozet	46°26′S	Oct 2011	KPA02	2.04	2.19	2.12	1.51	2.47	0.70	1.92	-0.13	1.34	-0.05	1.54	-21.57	10.10
King penguin	Crozet	46°26′S	Oct 2011	KPA03	1.63	1.73	2.24	1.48	2.49	0.71	2.01	0.02	1.38	-0.03	1.64	-22.12	9.95
King penguin	Crozet	46°26′S	Oct 2011	KPA04	1.73	1.87	2.29	1.52	2.52	0.79	2.02	0.02	1.37	0.03	1.64	-22.31	9.82
King penguin	Crozet	46°26′S	Oct 2011	KPA05	1.96	2.12	1.85	1.28	2.37	0.61	1.87	-0.06	1.40	-0.03	1.55	-21.32	10.07
King penguin	Crozet	46°26′S	Oct 2011	KPA06	1.80	1.90	2.17	1.59	2.60	0.76	1.97	-0.20	1.41	-0.03	1.57	-21.88	10.21
King penguin	Crozet	46°26′S	Oct 2011	KPA07	2.44	2.60	2.14	1.53	2.50	0.78	1.98	-0.16	1.35	0.01	1.59	-21.50	10.05
King penguin	Crozet	46°26′S	Oct 2011	KPA08	1.57	1.70	2.12	1.45	2.50	0.71	1.97	-0.04	1.41	-0.02	1.60	-21.96	9.76
King penguin	Crozet	46°26′S	Oct 2011	KPA09	1.91	2.02	2.12	1.40	2.38	0.71	1.96	0.03	1.33	0.00	1.61	-21.44	10.05
King penguin	Crozet	46°26′S	Oct 2011	KPA10	2.26	2.42	2.10	1.37	2.45	0.69	1.97	0.05	1.41	0.00	1.62	-21.24	10.32
King penguin	Crozet	46°26′S	Oct 2011	KPA11	1.65	1.77	2.33	1.64	2.61	0.77	2.07	-0.12	1.38	-0.06	1.65	-22.22	10.35
Macaroni penguin	Crozet	46°26′S	Jan 2012	MPA11	0.87	0.95	2.48	1.65	2.65	0.82	2.04	0.02	1.41	0.00	1.63	-19.60	8.16
Macaroni penguin	Crozet	46°26′S	Jan 2012	MPA12	1.05	1.09	2.59	1.73	2.69	0.90	2.00	0.01	1.39	0.03	1.57	-19.94	9.04
Macaroni penguin	Crozet	46°26′S	Jan 2012	MPA13	1.06	1.10	2.51	1.63	2.53	0.80	1.89	0.08	1.31	-0.02	1.48	-19.92	8.58
Macaroni penguin	Crozet	46°26′S	Jan 2012	MPA14	0.80	0.82	2.49	1.67	2.64	0.86	2.05	0.00	1.38	0.02	1.63	-19.79	8.79
Macaroni penguin	Crozet	46°26′S	Jan 2012	MPA15	0.91	0.95	2.31	1.60	2.52	0.81	1.94	-0.08	1.32	0.01	1.54	-19.44	8.62
Macaroni penguin	Crozet	46°26′S	Jan 2012	MPA16	0.89	0.92	2.61	1.74	2.63	0.90	1.97	0.00	1.32	0.03	1.53	-19.65	8.52

Macaroni penguin	Crozet	46°26′S	Jan 2012	MPA17	0.99	1.03	2.45	1.59	2.53	0.81	1.94	0.08	1.34	0.01	1.54	-19.57	8.26
Macaroni penguin	Crozet	46°26′S	Jan 2012	MPA18	1.16	1.25	2.41	1.61	2.55	0.72	1.88	0.01	1.34	-0.09	1.48	-19.45	8.00
Macaroni penguin	Crozet	46°26′S	Jan 2012	MPA19	1.13	1.18	2.23	1.49	2.40	0.71	1.84	0.01	1.28	-0.04	1.47	-21.89	9.10
Macaroni penguin	Crozet	46°26′S	Jan 2012	MPA20	1.29	1.34	2.80	1.88	2.83	0.95	2.05	-0.01	1.41	0.00	1.57	-20.59	8.48
Eastern rockhopper penguin	Crozet	46°26′S	Feb 2012	ERPA11	0.80	0.84	2.57	1.67	2.72	0.89	2.13	0.07	1.46	0.05	1.71	-20.16	8.53
Eastern rockhopper penguin	Crozet	46°26′S	Feb 2012	ERPA12	0.74	0.78	2.92	2.00	3.13	1.00	2.45	-0.06	1.63	0.00	1.95	-20.33	8.78
Eastern rockhopper penguin	Crozet	46°26′S	Feb 2012	ERPA13	1.04	1.12	3.04	2.00	3.06	1.05	2.27	0.06	1.56	0.05	1.77	-20.78	8.84
Eastern rockhopper penguin	Crozet	46°26′S	Feb 2012	ERPA14	1.07	1.13	3.00	2.01	3.08	1.05	2.34	-0.01	1.57	0.04	1.83	-20.93	8.75
Eastern rockhopper penguin	Crozet	46°26′S	Feb 2012	ERPA15	0.89	0.93	2.74	1.89	2.99	0.96	2.35	-0.08	1.57	0.01	1.87	-21.02	8.08
Eastern rockhopper penguin	Crozet	46°26′S	Feb 2012	ERPA16	1.34	1.39	3.22	2.12	3.05	1.08	2.18	0.06	1.46	0.01	1.65	-20.89	9.29
Eastern rockhopper penguin	Crozet	46°26′S	Feb 2012	ERPA17	1.00	1.03	3.04	2.05	3.09	1.03	2.26	-0.02	1.54	0.00	1.74	-21.12	8.64

Eastern rockhopper penguin	Crozet	46°26′S	Feb 2012	ERPA 18	0.87	0.89	3.10	2.12	3.05	0.93	2.09	-0.07	1.45	-0.13	1.55	-20.93	8.64
Eastern rockhopper penguin	Crozet	46°26′S	Feb 2012	ERPA 19	0.78	0.81	2.78	1.81	2.79	0.89	2.12	0.08	1.42	-0.02	1.67	-20.99	8.23
Eastern rockhopper penguin	Crozet	46°26′S	Feb 2012	ERPA 20	0.73	0.77	2.45	1.61	2.90	0.93	2.32	0.05	1.69	0.12	1.91	-21.03	7.79
Northern rockhopper penguin	Amsterdam	37°50′S	Nov 2011	NRPA 11	2.11	2.90	3.28	2.19	3.15	1.10	2.32	0.01	1.50	0.00	1.77	-18.86	10.11
Northern rockhopper penguin	Amsterdam	37°50′S	Nov 2011	NRPA 12	1.38	2.20	2.91	1.99	3.19	1.00	2.54	-0.05	1.70	0.00	2.04	-19.29	8.89
Northern rockhopper penguin	Amsterdam	37°50′S	Nov 2011	NRPA 13	1.68	1.83	2.87	1.91	3.02	1.02	2.49	0.02	1.59	0.06	2.00	-18.75	10.85
Northern rockhopper penguin	Amsterdam	37°50′S	Nov 2011	NRPA 14	2.42	3.50	3.19	2.14	3.06	1.14	2.33	-0.01	1.45	0.06	1.79	-19.14	10.23
Northern rockhopper penguin	Amsterdam	37°50′S	Nov 2011	NRPA 15	1.46	1.62	3.01	2.11	3.22	1.08	2.49	-0.14	1.64	0.02	1.95	-18.93	10.36
Northern rockhopper penguin	Amsterdam	37°50′S	Nov 2011	NRPA 16	2.19	2.32	3.44	2.28	3.27	1.23	2.46	0.03	1.55	0.08	1.89	-19.17	9.95
Northern rockhopper penguin	Amsterdam	37°50′S	Nov 2011	NRPA 17	1.48	2.20	3.15	2.08	3.12	1.16	2.51	0.05	1.56	0.12	1.99	-18.89	10.33

Northern rockhopper penguin	Amsterdam	37°50′S	Nov 2011	NRPA 18	2.51	2.77	3.63	2.32	3.28	1.33	2.57	0.16	1.53	0.17	1.98	-19.17	10.17
Northern rockhopper penguin	Amsterdam	37°50′S	Nov 2011	NRPA 19	1.84	2.01	3.45	2.37	3.38	1.14	2.44	-0.09	1.60	-0.05	1.84	-18.89	10.46
Northern rockhopper penguin	Amsterdam	37°50′S	Nov 2011	NRPA 20	2.41	2.59	3.19	2.17	3.02	1.11	2.23	-0.05	1.39	0.02	1.69	-19.13	9.70

Section 2. Calculation procedures of the Hg isotopic fractionation extent due to biogeochemical processes

Estimation of the fraction of photodemethylated MeHg in surface waters at distant sites of the Southern Ocean

The variations in the surface ocean MeHg photodemethylation can be estimated from the odd-MIF values recorded in seabird blood based on a Rayleigh model:

$$\ln\frac{1000+\Delta}{1000+\Delta i} = \frac{\varepsilon(\Delta^{199}Hg)}{1000} \times \ln(f) \quad (1)$$

where $\Delta^{199}Hg_i$ corresponds to the initial odd-MIF of the marine MeHg before undergoing photodemethylation, which was assumed to be close to zero based on the negligible total Hg Δ^{199}Hg values previously measured in seawater (Štrok et al., 2015). MeHg is also assumed to have a similar odd-MIF than the total Hg before photodemethylation because it is likely converted from inorganic Hg (Hg(II)) in the photic zone of the water column. The $\varepsilon(\Delta^{199}Hg)$ is the enrichment factor, reported as $\varepsilon = 1000*(\alpha_{\Delta 199Hg} - 1)$ as a function of the kinetic fractionation factor ($\alpha_{\Delta 199H}$) determined in laboratory experiments. f is the remaining fraction of non-photodemethylated MeHg.

The experimental estimations of the enrichment factors of MeHg aquatic photodemethylation were first calculated as a function of the MeHg/dissolved organic carbon (DOC) ratio by Bergquist and Blum, (2007). The relation between the odd-MIF values and the fraction of the remaining MeHg was used in fish from the Lake Michigan to estimate the MeHg photodegradation extent. This reference fractionation model was later applied for the estimation of the MeHg loss due to photodemethylation in marine environments (Gehrke et al., 2011; Point et al., 2011; Senn et al., 2010). Point et al. (2011) extrapolated the fractionation model to the presence of DOC in Arctic marine natural waters (lower DOC content) (Point et al., 2011). In a recent study, Chandan et al. (2015) investigated the Hg isotopic fractionation factors considering changing DOC binding sites and concluded that the odd-MIF extent is strongly dependent on the amount of reduced sulfur content in organic matter (Sred-DOC). The enrichment factors were evaluated under different types and concentrations of organic matter standards: Suwanee River fulvic acid (SRFA), Pony Lake fulvic acid (PL FAR) and Nordic Lake natural organic matter (NL NOM). These two reference organic matter models present contrasted proportions of reduced sulfur organic matter (35% for SRFA, 59% for PL FAR and 50% for NL NOM). Furthermore, these models represent more realistic environmental conditions (low MeHg: Sred-DOC ratios) than previous experimental studies and can be more representative of the processes occurring under natural conditions in the environment.

In order to estimate the extent of photochemical demethylation of MeHg over the studied sites of the Southern Ocean, we calculated the corresponding enrichment factors by

application of experimental models in our own environmental conditions of MeHg:DOC and MeHg: S red-DOC. The assessment was based on the three mentioned experimental studies: in mid-range MeHg: S-red-DOM ratio (SRFA) and low MeHg: S-red-DOM ratio (NL NOM) conditions (Chandan et al., 2015) and in function of MeHg:DOC ratios under high DOC conditions (Bergquist and Blum, 2007). The MeHg and DOC concentrations at each site were extracted from published data (

Table S5, Table S6 and Table S7). As previously explained, the concentrations of DOC in surface waters were not considered because photochemical reactions are known to photodegrade the organic matter. Moreover, MeHg is mainly produced at the bottom or below the photic zone, where plankton material is undergoing bacterial degradation and mineralization (Mason et al., 2012). We therefore extrapolated the isotopic fractionation systems of these three experimental models to our conditions of MeHg: S-red-DOC ratios and MeHg:DOC ratios by fitting equations for the three sites (Antarctic, subantarctic and subtropical zones). We obtained that the difference on the extent of photodemethylated MeHg from Antarctic and subantarctic to subtropical zones was in the order of 2%, independently of the experimental model used. When we considered the mid-range MeHg: Sred-DOC, the extent of photodemethylated MeHg varied from ~ 9% in Antarctic to ~ 11% in subtropical zones. Under low MeHg: Sred-DOC conditions, ~ 5% of MeHg was photodemthylated in Antarctic waters whereas ~ 6% in subtropical waters. The photodemethylated MeHg corresponding to MeHg-DOC ratios varied from ~ 13% in the Antarctic zones to 18% in the subtropics (Table S). No substantial changes in the latitudinal variations were observed in the calculated results when changing the mentioned parameters for all the empirical models used here. Previously calculated degrees of photodemethylation in Antarctic coastal ecosystems by the same experimental approximation were similar to our findings (Zheng et al., 2015). Also, Blum et al., (2013) found that the Δ^{199}Hg values of the MeHg at mesopelagic depth in the Pacific Ocean were about 1.5 - 2.0‰. These values are within the same range as our Δ^{199}Hg values, strongly suggesting that, since deep mixing in subtropical zones in the Southern Ocean occurs at >

400m depth, the MeHg accumulated in seabirds of the Southern oceanic Regions has a mesopelagic origin.

Table S5. Calculation of the MeHg:Sred-DOC ratios for the estimation of MeHg photodemethylation based on experimental fractionation factors (Chandan et al., 2015) for mid-range MeHg:Sred-DOC, SRFA organic matter conditions, 35% S-red).

		Reference data for this study[1]	Other published data[2]	Reference data [3]	Reference data[4]				
Zone	Depth	MeHg (pmol L^{-1})	MeHg (pmol L^{-1})	DOC (mg L^{-1})	DOS min (µmol L^{-1})	S org (%)	S red (%)	S red (mg L^{-1})	MeHg/S red-DOC (pg mg^{-1})
Antarctic Zone	0-100	0.21	0.05	0.60	0.19	0.010	0.0035	0.0021	0.021
	100-200	0.15	0.08	0.54	0.19	0.011	0.0039	0.0023	0.014
	200-500	0.15	0.05	0.48	0.19	0.013	0.0044	0.0020	0.016
Subantartic Zone	0-100	0.08	0.74	0.17	0.19	0.036	0.0043	0.0125	0.024
	100-200	0.11	0.33	0.48	0.19	0.013	0.0043	0.0044	0.011
	200-500	0.10	0.42	0.58	0.19	0.010	0.0043	0.0037	0.009
Subtropical Zone	0-100	0.08	0.05	0.39	0.19	0.016	0.0043	0.0055	0.013
	100-200	0.10	0.05	0.43	0.19	0.014	0.0043	0.0049	0.012
	200-500	0.10	0.05	0.52	0.19	0.012	0.0043	0.0041	0.010

[1] *Cossa et al. 2011*
[2] *AZ: Nerentorp Mastromonaco et al. 2017; SAZ: Canario et al. 2017; STZ: Bratkic et al. 2016*
[3] *Tremblay et al. 2015; Canario et al. 2017; Ogawa et al., 1999*
[4] *Ksionzek et al. 2016*

Table S6. Calculation of the MeHg:Sred-DOC ratios for the estimation of MeHg photodemethylation based on experimental fractionation factors (Chandan et al., 2015) for low-range MeHg:Sred-DOC, NL NOM organic matter conditions, 50% S-red).

		Reference data for this study[1]	Other published data[2]	Reference data [3]	Reference data[4]				
Zone	Depth	MeHg (pmol L^{-1})	MeHg (pmol L^{-1})	DOC (mg L^{-1})	DOS min (µmol L^{-1})	S org (%)	S red (%)	S red (mg L^{-1})	MeHg/S red-DOC (pg mg^{-1})
Antarctic Zone	0-100	0.21	0.05	0.6	0.19	0.010	0.0051	0.0030	0.014
	100-200	0.15	0.08	0.54	0.19	0.011	0.0056	0.0033	0.009
	200-500	0.15	0.05	0.48	0.19	0.013	0.0063	0.0029	0.010
Subantarctic Zone	0-100	0.08	0.74	0.17	0.19	0.036	0.0179	0.0010	0.155
	100-200	0.11	0.33	0.48	0.19	0.013	0.0063	0.0029	0.055
	200-500	0.10	0.42	0.58	0.19	0.010	0.0052	0.0035	0.045
Subtropical Zone	0-100	0.08	0.05	0.39	0.19	0.016	0.0078	0.0024	0.008
	100-200	0.10	0.05	0.43	0.19	0.014	0.0071	0.0026	0.008
	200-500	0.10	0.05	0.52	0.19	0.012	0.0058	0.0032	0.006

[1] *Cossa et al. 2011*
[2] *AZ: Nerentorp Mastromonaco et al. 2017; SAZ: Canario et al. 2017; STZ: Bratkic et al. 2016*
[3] *Tremblay et al. 2015; Canario et al. 2017; Ogawa et al., 1999*
[4] *Ksionzek et al. 2016*

Table S7. Calculation of the MeHg: DOC ratios for the estimation of the MeHg photodemethylation based on experimental fractionation factors (Bergquist and Blum, 2007) for high MeHg:DOC conditions.

		Reference data for this study[1]	Other published data [2]	Reference data [3]	
Zone	Depth	MeHg (pmol L^{-1})	MeHg (pmol L^{-1})	DOC (mg L^{-1})	MeHg/DOC (pg mg^{-1})
Antarctic Zone	0-100	0.21	0.05	0.6	0.350
	100-200	0.15	0.08	0.54	0.278
	200-500	0.15	0.05	0.48	0.313
Subantarctic Zone	0-100	0.08	0.74	0.17	0.471
	100-200	0.11	0.33	0.48	0.208
	200-500	0.10	0.42	0.58	0.172
Subtropical Zone	0-100	0.08	0.05	0.39	0.256
	100-200	0.10	0.05	0.43	0.233
	200-500	0.10	0.05	0.52	0.192

[1] *Cossa et al. 2011*
[2] *AZ: Nerentorp Mastromonaco et al. 2017; SAZ: Canario et al. 2017; STZ: Bratkic et al. 2016*
[3] *Tremblay et al. 2015; Canario et al. 2017; Ogawa et al., 1999*

Table S8. Estimation of the MeHg photodemethylation extent based on experimental fractionation factors (Bergquist and Blum, 2007) for the different MeHg:DOC or MeHg-Sred/DOC calculated ratios.

			Mid-range MeHg:Sred-DOC ratio *Chandan et al., 2015*	Low MeHg:Sred-DOC ratio *Chandan et al., 2015*	Low MeHg:DOC ratio *Bergquist and Blum, 2007*
Zone	Site	Seabird species	MeHg photodemethylation (%)	MeHg photodemethylation (%)	MeHg photodemethylation (%)
Antarctic Zone	Adélie Land	Antarctic skuas	9.5±0.5	4.9±0.5	14.5±2.3
	Adélie Land	Emperor penguins	7.2±0.7	3.7±0.4	12.9±1.2
	Adélie Land	Adélie penguins	9.7±0.6	5.0±0.3	15.7±1.1
Subantarctic Zone	Kerguelen	Brown skuas	9.5±0.3	4.9±0.2	17.9±0.6
	Crozet	Brown skuas	9.7±0.5	5.1±0.3	18.8±1.1
	Crozet (Polar Front)	King penguins	9.4±0.2	4.9±0.1	14.7±0.3
	Crozet	Gentoo penguins	8.4±0.4	4.3±0.2	13.1±0.6
	Crozet	Macaroni penguins	9.1±0.3	4.7±0.2	14.3±0.5
	Crozet	Rockhopper penguins	9.3±0.8	4.9±0.4	16.2±1.1
Subtropical Zone	Amsterdam	Brown skuas	10.6±0.3	5.5±0.1	17.2±0.4
	Amsterdam	Northern rockhopper penguin	11.3±0.7	5.9±0.4	18.4±1.1

Estimation of the MDF enrichment factor associated to MeHg photodemethylation

In order to estimate the enrichment of MDF values associated to the calculated photodemethylation extent at each site, we performed a recalculation of the fractionation factor of δ^{202}Hg values (α (δ^{202}Hg)) for our environmental conditions. We based this calculation on the enrichment factors attributed to mid-range MeHg;S red-DOC (

Table **S**) and low MeHg;S red-DOC (Table S), which seem to be the closest model to our conditions in the Southern Ocean. We could estimate a α (δ^{202}Hg)/α (Δ^{199}Hg) near 1 in both cases (and both seabird models), meaning that during photodemethylation of MeHg, the same degree of fractionation is experienced by δ^{202}Hg and Δ^{199}Hg. Consequently, considering that the overall latitudinal MIF variations are attributed to MeHg photodemethylation and are in the order of 0.3‰ (~ 0.25‰ and ~ 0.32‰, respectively for skuas and penguins), we could explain ~ 0.3‰ of the total latitudinal MDF variations due to MeHg photodemethylation.

Table S9. Calculation of the fractionation factors of MDF (α (δ^{202}Hg)) corresponding to MeHg photodemethylation for each study area based on experimental studies under mid-range MeHg:Sred-DOC conditions (SRFA organic matter conditions, 35% S-red) (Chandan et al., 2015).

Conditions: mid-range MeHg;S red-DOC (35% S-red)					
Population/ Sites	ε Δ^{199}Hg (‰)	α (Δ^{199}Hg)	ε δ^{202}Hg (‰)	α (δ^{202}Hg)	Ratio α (δ^{202}Hg)/α (Δ^{199}Hg)
Skuas					
AZ	-5.23895	0.99476	-4.73312	0.99527	
SAZ	-5.24037	0.99476	-4.73440	0.99527	
STZ	-5.20641	0.99479	-4.70372	0.99530	1.00051
Penguins					
AZ	-5.30277	0.99470	-4.79078	0.99521	
SAZ	-5.26504	0.99473	-4.75669	0.99524	
STZ	-5.163113	0.99484	-4.66461	0.99534	1.00050

Table S10. Calculation of the fractionation factors of MDF (α (δ^{202}Hg)) corresponding to MeHg photodemethylation for each study area based on experimental studies under mid-range MeHg:Sred-DOC conditions (SRFA organic matter conditions, 35% S-red) (Chandan et al., 2015).

Conditions: low MeHg;S red-DOC (50% S-red)					
Population/ Sites	ε Δ^{199}Hg (‰)	α (Δ^{199}Hg)	ε δ^{202}Hg (‰)	α (δ^{202}Hg)	Ratio α (δ^{202}Hg)/α (Δ^{199}Hg)
Skuas					
AZ	-1.501006	0.998499	-1.520006	0.998480	
SAZ	-1.500575	0.998499	-1.519569	0.998480	
STZ	-1.495628	0.998504	-1.514560	0.998485	0.99998
Penguins					
AZ	-1.438243	0.998562	-1.456449	0.998544	
SAZ	-1.504152	0.998496	-1.523191	0.998477	
STZ	-1.489287	0.998511	-1.508138	0.998492	0.99998

Fractionation (MDF) involved during Hg^0 partitioning and equilibrium between water and air

Calculation of the Henry's law constant (K_H). The calculation of Henry's law constant permits to estimate the gaseous elemental Hg partition at equilibrium between water and air as a function of the water surface temperature. This constant represents the fraction of gaseous Hg^0 as a function of the Hg^0 remaining in the aqueous phase.

(2)

$$K_{H'} = \frac{[Hg^0]_{(g)}}{[Hg^0]_{(aq)}}$$

An equation for artificial sea water (concentration conditions of 1.5 M of NaCl) proposed by (Andersson et al., 2008).

(3)

$$K_{H'} = e\left(\frac{-1871.6}{T\,(K)}\right) + 5.28$$

The data of water temperature were taken from previous studies in austral autumn (Cossa et al., 2011) and summer (Canario et al., 2017). Based on the approximate values of temperature surface water, we estimated the yearly volatilization extents taking place at each site. The obtained values were K_H = 0.21 (T = 273 K), 0.25 (T = 281 K) and 0.32 (T = 291 K) respectively for the Antarctic, the subantarctic and the subtropical zones.

Calculation of the kinetic fractionation factor α($^{198}Hg/^{202}Hg$) as a function of the Hg remaining fraction (f_R) at each latitude. The Hg remaining fraction (f_R) was calculated from the water/air partitioning constant K_H in order to estimate the Hg fractionation magnitude during volatilization at each location. The experimental volatilization of aqueous Hg^0 into gaseous Hg^0 indicated a MDF with a low kinetic fractionation factor α($^{198}Hg/^{202}Hg$). The obtained during experimental volatilization process was similar for accumulative fractionation (1.00044) and instantaneous fractionation (1.00047), indicating that Hg isotopic fractionation during volatilization is independent of the initial solution volumes and the volatilization rates (Zheng et al., 2007). According to this volatilization experiment, we calculated the α($^{198}Hg/^{202}Hg$) from the slope when plotting log(1000-δf/1000-δi) vs log(f_R) following this equation:

(4)

$$\log\left(\frac{1000-\delta}{1000-\delta i}\right)=\left(\frac{1}{\alpha}-1\right)\times\log(f_R)$$

where δ is the isotopic composition of the remaining reactant at time t, δi is the initial isotopic composition of the reactant, f_R is the fraction of the remaining reactant at time t, and α is the kinetic fractionation factor.

Based on experimental calculations, we determined the Rayleigh-type fractionation slope for our model, assuming that initial $\delta^{202}Hg$ (δ_i) is 0 and taking α($^{198}Hg/^{202}Hg$) of 1.00047

(Zheng et al., 2007) (Table S). The obtained slope represents a $\alpha(^{198}Hg/^{202}Hg)$ factor of 1.0005, meaning a total mass-dependent fractionation of 0.03 ‰ due to volatilization (i.e. kinetic fractionation between seawater and air).

Table S11. Calculation of the volatilised fraction of Hg and the MDF enrichment factor ($\delta^{202}Hg$) corresponding to Hg volatilisation following the Henry's law constant value and the Hg isotopic fractionation models during experimental volatilisation processes.

Site	Water temperature *(K)*	Henry's constant (K_H)	Conc Hg^0 (air) *(ng m^{-3})* (1)	Calculated Eq. Hg^0 (aq) *(ng m^{-3})*	f_R (Hg^0 aq)	log (f_R)	ε $\delta^{202}Hg$ *(‰)*
AZ	273	0.21	0.93	4.50	0.829	-0.188	0.088
SAZ	281	0.25	0.90	3.58	0.799	-0.224	0.105
STZ	291	0.31	1.03	3.32	0.763	-0.270	0.127

(1) AZ: Pfaffhuber et al. 2012 ; SAZ: ; STZ :Angot et et al. 2014

Estimation of the "biogenic" MDF enrichment associated to the extent of microbial transformation processes (reduction and net methylation) at the different sites

In order to explain the Hg MDF enrichment observed in the studied latitudinal gradient, we suggested the existence of potential differences in the extent of biological processes (only inducing MDF) between sites. For the estimation of these potential differences, we related the difference of MDF fractionation extent between Antarctic and subtropical zones, here $\Delta(\delta^{202}Hg)$, to the ratio of the remaining reactant Hg fraction (f_R) between both sites by applying the following equation:

(5)

$$\Delta(\delta^{202}Hg) = \delta^{202}Hg_{STZ} - \delta^{202}Hg_{AZ}$$

$$= 1000 \times e^{\log\left(\frac{1000-\delta^{202}Hg_{STZ}}{1000}\right)} - 1000 \times e^{\log\left(\frac{1000-\delta^{202}Hg_{AZ}}{1000}\right)}$$

$$\Delta(\delta^{202}Hg) = \left(\frac{1}{\quad} - 1\right) \times \log(f_{\quad}) \qquad \left(\frac{1}{\quad} - 1\right) \times \log(f_{\quad})$$

The remaining fraction (f_R) calculated at the respective sites corresponds to:

$$f_R = 1 - \frac{(Hg_f)}{(Hg_i)}$$

Considering similar conditions of Hg bioavailability between both sites ($Hg_{i,AZ} \sim Hg_{i,STZ}$), we directly related the remaining reactant Hg fraction to the concentration of the produced Hg fraction (Hg_f) between sites:

(6)

$$\log\left(\frac{(f_R)_{STZ}}{(f_R)_{AZ}}\right) \sim \frac{(Hg_f)_{STZ}}{(Hg_f)_{AZ}}$$

MDF enrichment estimated for biological reduction of Hg. For the estimation of the difference in magnitude of Hg(II) reduction between the Antarctic and the subtropical zones, we based on the experimental kinetic fractionation factor $\alpha(^{198}Hg/^{202}Hg)$ obtained during biological reduction experimental studies (Kritee et al., 2007, 2008). In these previous studies, Hg isotopic fractionation was first measured during Hg reduction by Hg-resistant bacteria expressing the mercuric reductase (merA) enzyme. This process induces Hg MDF leaving the remaining inorganic fraction enriched in heavy isotopes and defining a Rayleigh system with an associated kinetic fractionation factor $\alpha(^{198}Hg/^{202}Hg)$ ranging between 1.0013 and 1.0020 (meaning a $\delta^{202}Hg$ enrichment of Hg(0) between -1.3‰ and -2.0‰) (Kritee et al., 2007). Similar results were obtained during biological reduction by two Hg-resistant strains (-1.6‰) and the MDF fractionation obtained by Hg-sensitive strain without the enzyme merA (-0.4‰) (Kritee et al., 2008). Considering these kinetic fractionation factors $\alpha(^{198}Hg/^{202}Hg)$, we estimated that, to explain a total latitudinal MDF enrichment between 1.0 and 1.5‰, the extent of biological reduction in subtropical waters

should be around 1.65 to 3.18 times higher in subtropical waters than in Antarctic waters for Hg-resistant bacteria and until 40 times higher in the case of un-resistant bacteria (

Table S). Considering that the natural bacteria are not adapted to high Hg concentrations, the reduction by Hg-sensitive bacteria without merA enzyme may be more representative of marine ecosystems. However, these potential isotopic fractionation pathways directly affect the Hg(II) isotopic baseline mainly in the euphotic zone, while MeHg isotopic baseline will be more directly affected by methylation and demethylation pathways in both the euphotic and the mesopelagic zones. Consequently, such estimations obtained for Hg(II) reduction/volatilization mechanisms do not preclude for any solid conclusion regarding the latitudinal MDF variations of MeHg. Most importantly, the impact on MDF of Hg of biogenic processes leading to the net methylation/demethylation of Hg must be explored and evaluated.

Estimation of the MDF enrichment associated to the extent of MeHg microbial net methylation at different latitudes. We wanted to estimate the difference of net "apparent" Hg methylation associated to the observed MDF enrichment between latitudes. We refer to the term "apparent" methylation because methylation and demethylation occur simultaneously so that the product of the reaction (MeHg) would be converted back to the reactant (Hg(II)). During microbial demethylation, the lighter Hg isotopes of the MeHg molecules are preferentially transformed and have been found to influence the Hg isotopic composition when significant amounts of MeHg are accumulated (Pedrero et al., 2012). We based our calculations on two experimental model by sulphate reducing bacteria (SRB) under sulphate respiration conditions (Perrot et al., 2015) and abiotic methylation/demethylation by methylcobalamin (MeCo) (Jiménez-Moreno et al., 2013).

The associated kinetic fractionation factor $\alpha(^{198}Hg/^{202}Hg)$ were, respectively, 1.0025 and 1.0016. During these experiments, a steady-state between the Hg(II) and MeHg isotopic composition was observed after 24 h of experiment. It was demonstrated that the occurrence of significant simultaneous demethylation would lead to uncertainty in the modelled fractionation factor since lighter Hg isotopes of MeHg would be preferentially demethylated. These experiments were conducted in closed system allowing reversible reaction to occur (methylation/demethylation). Under these conditions two opposite Rayleigh distillation system are in competition, and probably represent a better approximation of such antagonistic and simultaneous mechanisms involved in specific methylating niches of the marine water column (oxygen minimum, pycnocline or maximum planktonic biomass) (Sunderland et al., 2009; Cossa et al., 2011). This assumption implies that MeHg is biogenically produced in confined media or at very specific location in the pelagic zone to avoid any effect from turbulent diffusion or vertical advection.

The difference of MDF fractionation between the Antarctic and the subtropical zones was related to the ratio of produced MeHg (Hg_f) fraction between sites with equation (6). For the explanation of a total MDF enrichment between 1.0 and 1.5‰ between sites, we obtained that the net methylation extent in subtropical waters might be around 1.5 to 2.5 times higher than in Antarctic waters (Table S). The obtained variability for MeHg net formation between Antarctic and subtropical marine waters seems quite reasonable. The two different and productive pelagic systems have a substantial temperature difference (0

ºC to 18 ºC in the photic zone from Antarctic to subtropical waters) that can dramatically control bacterial activities towards a higher net production of MeHg in subtropical waters. This also provides an additional explanation for the higher bioaccumulation of MeHg in seabirds moving northward.

Table S12. Calculation of the fraction of reduced Hg between the studied sites considering theoretical kinetic fractionation factors.

Hg(II) reduction (aq)- Hg-resistant bacteria merA			
α δ^{202}Hg (‰)	1.0013		
Kritee et al., 2007			
$\Delta(\delta^{202}Hg)$	log (fR_{STZ}/fR_{AZ})	fR_{STZ}/fR_{AZ}	conc $[MeHg]_{STZ}/[MeHg]_{AZ}$
2	-0.8020	0.4484	2.23
1.50	-1.16	0.31	3.18
1.00	-0.77	0.46	2.16
Hg(II) reduction (aq)- Hg-resistant bacteria merA			
α δ^{202}Hg (‰)	1.002		
Kritee et al., 2007			
$\Delta(\delta^{202}Hg)$	log (fR_{STZ}/fR_{AZ})	fR_{STZ}/fR_{AZ}	conc $[MeHg]_{STZ}/[MeHg]_{AZ}$
1.50	-0.75	0.47	2.12
1.00	-0.50	0.61	1.65
Hg(II) bacterial reduction (aq)- Hg-sensitive bacteria (no mer system)			
α δ^{202}Hg (‰)	1.0004		
Kritee et al., 2008			
$\Delta(\delta^{202}Hg)$	log (fR_{STZ}/fR_{AZ})	fR_{STZ}/fR_{AZ}	conc $[MeHg]_{STZ}/[MeHg]_{AZ}$

1.5	-3.75	0.02	42.6
1.00	-0.63	0.53	1.87
Hg(II) bacterial reduction (aq)- Hg-resistant			
α δ^{202}Hg (‰)	1.0016		
Kritee et al., 2008			
$\Delta(\delta^{202}Hg)$	log (fR_{STZ}/ fR_{AZ})	fR_{STZ}/ fR_{AZ}	conc $[MeHg]_{STZ}$/$[MeHg]_{AZ}$
1.50	-0.94	0.39	2.56
1.00	-0.63	0.53	1.87

Table S13. Calculation of the fraction of methylated Hg between the studied sites considering theoretical kinetic fractionation factors.

Hg(II) net bacterial methylation (aq)- sulphate respiration			
α δ^{202}Hg (‰)	1.0025	*Perrot et al., 2015*	
$\Delta(\delta^{202}Hg)$	log ($f_{R\ STZ}$/ $f_{R\ AZ}$)	$f_{R\ STZ}$/ $f_{R\ AZ}$	[MeHg] $_{STZ}$/[MeHg] $_{AZ}$
1.50	-0.60	0.55	1.82
1.00	-0.40	0.67	1.49
Hg(II) net abiotic methylation (aq) by MeCo			
α δ^{202}Hg (‰)	1.0016	*Jiménez Moreno et al., 2013*	
$\Delta(\delta^{202}Hg)$	log ($f_{R\ STZ}$/ $f_{R\ AZ}$)	$f_{R\ STZ}$/ $f_{R\ AZ}$	[MeHg] $_{STZ}$/[MeHg] $_{AZ}$
1.50	-0.94	0.39	2.56
1.00	-0.63	0.53	1.87

Table S14. Details of sample collection periods and phytoplankton bloom periods in each study area during austral summer 2011-2012.

Species	Location	Latitude	Sampling	Bloom period
South polar skua	Adélie Land	66°40'S	December 2011 /January 2012	January/February
Adélie penguin	Adélie Land	66°40'S	February 2012	January/February
Brown skua	Kerguelen	49°21′S	December 2011	November/December
Brown skua	Crozet	46°26′S	January/February 2012	November/December
King penguin	Crozet	46°26′S	October 2012	November/December
Macaroni penguin	Crozet	46°26′S	January 2012	November/December
Eastern rockhopper penguin	Crozet	46°26′S	February 2012	November/December
Brown skua	Amsterdam	37°50′S	December 2011	October
Northern rockhopper penguin	Amsterdam	37°50′S	November 2011	October

Section 3. Additional information on ecological characteristics of seabird species

The diet of skua chicks is usually composed of other birds and marine mammals scavenge or seabird eggs, and also of fish when feeding at sea. Depending on the location, skuas present different feeding ecologies. South polar skuas from Adélie Land feed their chick with eggs and carcasses of Adélie penguins *Pygoscelis adeliae* (Carravieri et al., 2017). In the Kerguelen Islands, skua diet is particularly composed of blue petrels *Halobaena caerulea* and thin-billed prions, *Pachyptila belcheri* (Mougeot et al., 1998). Crozet skuas rely mainly on eggs and carcasses of crested penguins (*Eudyptes chrysolophus* and *E. chrysocome filholi*), but also on black rats *Rattus rattus* that were introduced by humans. In Amsterdam Island, skua diet is not completely recognized but, according to field observations, chicks are fed with other seabird eggs and carcasses and with Antarctic fur seals *Arctocephalus tropicalis* scavenge, but also with the introduced subantarctic rats *Rattus norvegicus* (Carravieri et al., 2017).

We studied penguin adult individuals from five species: king penguin *Aptenodytes patagonicus*, Adélie *Pygoscelis adeliae*, macaroni *Eudyptes chrysolophus*, eastern rockhopper *E. chrysocome filholi* and northern rockhopper *E. chrysocome moseleyi* penguins. King penguins mainly feed on pelagic fish, especially myctophids such as *Krefftichthys anderssoni* (Bost et al., 2002; Cherel et al., 2010). Adélie penguins also consume fish but their diet is mostly composed of krill (especially, *Euphausia superba* and *E. crystallorophias*) (Rodary et al., 2000b). Macaroni penguins primarily feed on crustaceans, such as hyperiids (e.g. *Themisto gaudichaudii*, and *Primno macropa*) and euphausiids (e.g. *E. vallentini*, *Thysanoessa* spp.), and on fish such as the myctophid *Krefftichthys anderssoni* (Cherel et al., 2010; Cherel and Hobson, 2007; Thiebot et al., 2014). Eastern rockhopper penguins from Crozet Islands are known to rely upon the

Antarctic krill *E. vallentini*, while northern rockhopper penguins from Amsterdam Island mainly feed on the euphasiid *Thysanoessa gregaria* and squid (Tremblay and Cherel, 2003). Chicks of emperor penguins (*Aptenodytes forsteri*) are winter breeders and were studied in order to evaluate the seasonal variations (summer vs winter) in the Antarctic continent. In winter, emperor penguins mainly feed over the Antarctic continental shelf and they present excellent diving capacities. They forage mainly on fish (and squids) of benthic areas between 200 and 400 m depth (Wienecke et al., 2007). Due to their seasonal mismatch relative to the other studied seabirds, they were not considered for the exploration of Hg isotopes at different latitudes.

Section 4. Supplemental discussion on temporal variability in odd-MIF values: winter and summer periods in Antarctic zone.

Antarctic ecosystems are characterized by contrasted annual insolation conditions between the dark period of the austral winter, when the sun does not rise above the horizon, and summertime when the day length accounts ~ 16 hours. As previously said, the photodemethylation of MeHg in surface waters is a major pathway for degradation of MeHg to Hg(II) and further photoreduction to Hg^0. For instance, a higher loss of MeHg by photodemethylation has been observed in open marine waters due to a greater penetration of light of all the wavelengths, especially UV light (i.e. UV-A and –B) which degrades MeHg more efficiently (DiMento and Mason, 2017). Due to the extreme sunlight conditions in Antarctic ecosystems during the year, we expected lower MeHg photodemethylation efficiency in the Antarctic waters (70° S) compared to northern latitudes (50 to 35° S). Indeed, the Antarctic seabird populations (Adélie penguins and South polar skua chicks) presented significantly lower mean Δ^{199}Hg values (1.52 ± 0.09‰) compared to subantartic (1.60 ± 0.14‰) and subtropical communities (1.82 ± 0.11‰), when we considered both the penguin and the skua populations together ($H = 39.29$, $p < 0.0001$). The Hg isotopic composition of the blood of both the chick and the adult penguins is representative of the recent Hg exposure before sampling, i.e., the breeding period (Renedo et al., 2018a). In the case of Adélie penguins and South polar skuas, this period corresponds to the summertime. Here, we compared the blood Hg isotopic values of these two summer breeder species with the blood Hg isotopic signatures of a winter breeder penguin inhabiting the Antarctic ecosystems, the emperor penguin, representative of the Antarctic winter period (Figure S). The significantly lower Δ^{199}Hg values of emperor penguins relative to the other two summer breeders (~ 0.5‰) could suggest that the bioaccumulated MeHg has undergone lower photodemethylation extent

in winter as a result of lower solar radiation and a potentially higher influence of sea ice cover, as already observed in previous studies in the Arctic (Masbou et al., 2015; Point et al., 2011). The sea ice coverage during sample collection in spring (November 2011) and summer (February 2012) was 10.8 x 10^6 km^2 and 2.2 x 10^6 km^2, respectively (National Snow and Ice Data Center (NSIDC)).

Because Hg odd-MIF varies as a function of the extent of light penetration at different depths of the water column, another potential contributor factor that could enhance the Δ^{199}Hg variations between Antarctic seabird populations is the different foraging habitat. Indeed, emperor penguins dive deep (until 400 m depth, as observed from satellite and dive tracking (Rodary et al., 2000a; Wienecke et al., 2007) and they forage in more neritic waters (as concluded from δ^{13}C signatures, Cherel, 2008). Previously observed Δ^{199}Hg differences between penguins with contrasted foraging depths and coastal *vs* open ocean feeders within a same community (Crozet Islands) accounted for less than 0.4‰ between epipelagic and benthic foragers (Renedo et al., 2018b). Based on this approach, the greater difference in Δ^{199}Hg values between Antarctic summer and winter breeders could be partly attributed to the difference in foraging depths between species. However, other factors that could explain the observed Hg odd-MIF trend are probably seasonal climatic differences such as the solar radiation and the sea ice coverage.

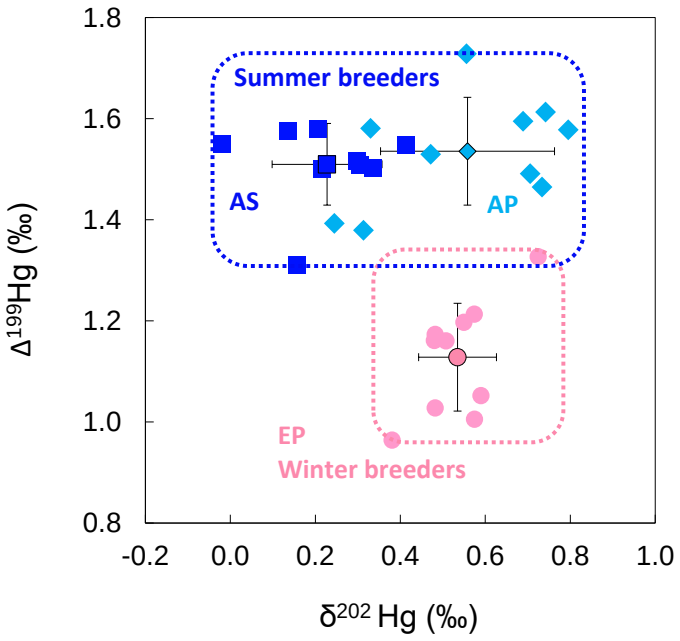

Figure S5. Odd-MIF differences between Antarctic winter and summer breeders. Hg isotopic composition (δ^{202}Hg, Δ^{199}Hg) of Antarctic seabirds, which are representative of both the summer period (AP: Adélie penguins, AS: Antarctic skua) and the winter period (EP: emperor penguins) of Adélie Land.

References

Andersson, M.E., Gårdfeldt, K., Wängberg, I., Strömberg, D., 2008. Determination of Henry's law constant for elemental mercury. Chemosphere 73, 587–592. https://doi.org/10.1016/j.chemosphere.2008.05.067

Angot, H., Barret, M., Magand, O., Ramonet, M., Dommergue, A., 2014. A 2-year record of atmospheric mercury species at a background Southern Hemisphere station on Amsterdam Island. Atmos. Chem. Phys. 14, 11461–11473. https://doi.org/10.5194/acp-14-11461-2014

Angot, H., Dion, I., Vogel, N., Legrand, M., Magand, O., Dommergue, A., 2016. Multi-year record of atmospheric mercury at Dumont d'Urville, East Antarctic coast: Continental outflow and oceanic influences. Atmos. Chem. Phys. 16, 8265–8279. https://doi.org/10.5194/acp-16-8265-2016

Bergquist, B.A., Blum, J.D., 2007. Mass-dependent and -independent fractionation of Hg isotopes by photoreduction in aquatic systems. Science 318, 417–20. https://doi.org/10.1126/science.1148050

Blum, J.D., Popp, B.N., Drazen, J.C., Anela Choy, C., Johnson, M.W., 2013. Methylmercury production below the mixed layer in the North Pacific Ocean. Nat. Geosci. 6, 879–884. https://doi.org/10.1038/ngeo1918

Bost, C.A., Zorn, T., Le Maho, Y., Duhamel, G., 2002. Feeding of diving predators and diel vertical migration of prey: King penguins' diet versus trawl sampling at Kerguelen Islands. Mar. Ecol. Prog. Ser. 227, 51–61. https://doi.org/10.3354/meps227051

Bratkic, A., Vahcic, M., Kotnik, J., Obu Vazner, K., Begu, E., Woodward, E.M.S., Horvat, M., 2016. Mercury presence and speciation in the South Atlantic Ocean along the 40°S transect. Global Biogeochem. Cycles 30, 105–119. https://doi.org/10.1002/2015GB005275

Canario, J., Santos-Echeandía, J., Koch, B.P., Laglera, L., 2017. Mercury and methylmercury in the Atlantic sector of the Southern Ocean. Deep. Res. Part II 138, 52–62. https://doi.org/10.1016/j.dsr2.2016.07.012

Carravieri, A., Cherel, Y., Brault-Favrou, M., Churlaud, C., Peluhet, L., Labadie, P., Bustamante, P., 2017. From Antarctica to the subtropics : Contrasted geographical concentrations of selenium , mercury , and persistent organic pollutants in skua chicks (Catharacta spp .). Environ. Pollut. 228, 464–473. https://doi.org/10.1016/j.envpol.2017.05.053

Chandan, P., Ghosh, S., Bergquist, B.A., 2015. Mercury isotope fractionation during aqueous photoreduction of monomethylmercury in the presence of dissolved organic matter. Environ. Sci. Technol. 49, 259–267.

https://doi.org/10.1021/es5034553

Chen, J., Hintelmann, H., Feng, X., Dimock, B., 2012. Unusual fractionation of both odd and even mercury isotopes in precipitation from Peterborough, ON, Canada. Geochim. Cosmochim. Acta 90, 33–46. https://doi.org/10.1016/j.gca.2012.05.005

Cherel, Y., 2008. Isotopic niches of emperor and Adélie penguins in Adélie Land, Antarctica. Mar. Biol. 154, 813–821. https://doi.org/10.1007/s00227-008-0974-3

Cherel, Y., Fontaine, C., Richard, P., Labat, J.-P., 2010. Isotopic niches and trophic levels of myctophid fishes and their predators in the Southern Ocean. Limnol. Oceanogr. 55, 324–332. https://doi.org/10.4319/lo.2010.55.1.0324

Cherel, Y., Hobson, K.A., 2007. Geographical variation in carbon stable isotope signatures of marine predators : a tool to investigate their foraging areas in the Southern Ocean. Mar. Ecol. Prog. Ser. 329, 281–287.

Cossa, D., Heimbürger, L.-E., Lannuzel, D., Rintoul, S.R., Butler, E.C.V., Bowie, A.R., Averty, B., Watson, R.J., Remenyi, T., 2011. Mercury in the Southern Ocean. Geochim. Cosmochim. Acta 75, 4037–4052. https://doi.org/10.1016/j.gca.2011.05.001

Demers, J.D., Blum, J.D., Zak, D.R., 2013. Mercury isotopes in a forested ecosystem: Implications for air-surface exchange dynamics and the global mercury cycle. Global Biogeochem. Cycles 27, 222–238. https://doi.org/10.1002/gbc.20021

DiMento, B.P., Mason, R.P., 2017. Factors controlling the photochemical degradation of methylmercury in coastal and oceanic waters. Mar. Chem. 196, 116–125. https://doi.org/10.1016/j.marchem.2017.08.006

Enrico, M., Roux, G. Le, Marusczak, N., Heimbürger, L.E., Claustres, A., Fu, X., Sun, R., Sonke, J.E., 2016. Atmospheric Mercury Transfer to Peat Bogs Dominated by Gaseous Elemental Mercury Dry Deposition. Environ. Sci. Technol. 50, 2405–2412. https://doi.org/10.1021/acs.est.5b06058

Gehrke, G.E., Blum, J.D., Marvin-DiPasquale, M., 2011. Sources of mercury to San Francisco Bay surface sediment as revealed by mercury stable isotopes. Geochim. Cosmochim. Acta 75, 691–705. https://doi.org/10.1016/j.gca.2010.11.012

Gionfriddo, C.M., Tate, M.T., Wick, R.R., Schultz, M.B., Zemla, A., Thelen, M.P., Schofield, R., Krabbenhoft, D.P., Holt, K.E., Moreau, J.W., 2016. Microbial mercury methylation in Antarctic sea ice. Nat. Microbiol. 1, 16127. https://doi.org/10.1038/nmicrobiol.2016.127

Gratz, L.E., Keeler, G.J., Blum, J.D., Sherman, L.S., 2010. Isotopic composition and fractionation of mercury in Great Lakes precipitation and ambient air. Environ. Sci. Technol. 44, 7764–70. https://doi.org/10.1021/es100383w

Jiménez-Moreno, M., Perrot, V., Epov, V.N., Monperrus, M., Amouroux, D., 2013. Chemical kinetic isotope fractionation of mercury during abiotic methylation of Hg(II) by methylcobalamin in aqueous chloride media. Chem. Geol. 336, 26–36. https://doi.org/10.1016/j.chemgeo.2012.08.029

Kritee, K., Blum, J.D., Barkay, T., 2008. Mercury Stable Isotope Fractionation during Reduction of Hg(II) by Different Microbial Pathways. Environ. Sci. Technol. 42, 9171–9177. https://doi.org/10.1021/es801591k

Kritee, K., Blum, J.D., Johnson, M.W., Bergquist, B.A., Barkay, T., 2007. Mercury stable isotope fractionation during reduction of Hg(II) to Hg(0) by mercury resistant microorganisms. Environ. Sci. Technol. 41, 1889–1895. https://doi.org/10.1021/es062019t

Ksionzek, K.B., Lechtenfeld, O.J., McCallister, S.L., Schmitt-Kopplin, P., Geuer, J.K., Geibert, W., Koch, B.P., 2016. Dissolved organic sulfur in the ocean: Biogeochemistry of a petagram inventory. Science (80-.). 354, 456–459. https://doi.org/10.1126/science.aaf7796

Li, M., Sherman, L.S., Blum, J.D., Grandjean, P., Mikkelsen, B., Weihe, P., Sunderland, E.M., Shine, J.P., 2014. Assessing sources of human methylmercury exposure using stable mercury isotopes. Environ. Sci. Technol. 48, 8800–8806. https://doi.org/10.1021/es500340r

Masbou, J., Point, D., Sonke, J.E., Frappart, F., Perrot, V., Amouroux, D., Richard, P., Becker, P.R., 2015. Hg stable isotope time trend in ringed seals registers decreasing sea ice cover in the Alaskan Arctic. Environ. Sci. Technol. 49, 8977–8985. https://doi.org/10.1021/es5048446

Mason, R.P., Choi, A.L., Fitzgerald, W.F., Hammerschmidt, C.R., Lamborg, C.H., Soerensen, A.L., Sunderland, E.M., 2012. Mercury biogeochemical cycling in the ocean and policy implications. Environ. Res. 119, 101–117. https://doi.org/10.1016/j.envres.2012.03.013

Mougeot, F., Genevois, F., Bretagnolle, V., 1998. Predation on burrowing petrels by the brown skua (Catharacta skua lo È nnbergi) at Mayes Island, Kerguelen. J. Zool. London 244, 429–438. https://doi.org/10.1017/S0952836998003136

National Snow and Ice Data Center (NSIDC), n.d. Antarctic sea ice extent 2011, 2012.

Nerentorp Mastromonaco, M.G., Gårdfeldt, K., Assmann, K.M., Langer, S., Delali, T., Shlyapnikov, Y.M., Zivkovic,

I., Horvat, M., 2017. Speciation of mercury in the waters of the Weddell, Amundsen and Ross Seas (Southern Ocean). Mar. Chem. 193, 20–33. https://doi.org/10.1016/j.marchem.2017.03.001

Obrist, D., Agnan, Y., Jiskra, M., Olson, C.L., Dominique, P., Hueber, J., Moore, C.W., Sonke, J., Helmig, D., 2017. Tundra uptake of atmospheric elemental mercury drives Arctic mercury pollution. Nat. Publ. Gr. 547, 201–204. https://doi.org/10.1038/nature22997

Ogawa, H., Fukuda, R., Koike, I., 1999. Vertical distributions of dissolved organic carbon and nitrogen in the Southern Ocean. Deep. Res. I 46, 1809–1826. https://doi.org/10.1016/S0967-0637(99)00027-8

Pedrero, Z., Bridou, R., Mounicou, S., Guyoneaud, R., Monperrus, M., Amouroux, D., 2012. Transformation, localization, and biomolecular binding of Hg species at subcellular level in methylating and nonmethylating sulfate-reducing bacteria. Environ. Sci. Technol. 46, 11744–51. https://doi.org/10.1021/es302412q

Perrot, V., Bridou, R., Pedrero, Z., Guyoneaud, R., Monperrus, M., Amouroux, D., 2015. Identical Hg isotope mass dependent fractionation signature during methylation by sulfate-reducing bacteria in sulfate and sulfate-free environment. Environ. Sci. Technol. 49, 1365–1373. https://doi.org/10.1021/es5033376

Pfaffhuber, K.A., Berg, T., Hirdman, D., Stohl, A., 2012. Atmospheric mercury observations from Antarctica: Seasonal variation and source and sink region calculations. Atmos. Chem. Phys. 12, 3241–3251. https://doi.org/10.5194/acp-12-3241-2012

Point, D., Sonke, J.E., Day, R.D., Roseneau, D.G., Hobson, K.A., Pol, S.S. Vander, Moors, A.J., Pugh, R.S., Donard, O.F.X., Becker, P.R., 2011. Methylmercury photodegradation influenced by sea-ice cover in Arctic marine ecosystems. Nat. Geosci. 4, 1–7. https://doi.org/10.1038/ngeo1049

Renedo, M., Amouroux, D., Cherel, Y., Bustamante, P., 2018a. Identification of sources and bioaccumulation pathways of MeHg in subantarctic penguins : a stable isotopic investigation. Sci. Rep. 1–10. https://doi.org/10.1038/s41598-018-27079-9

Renedo, M., Amouroux, D., Duval, B., Carravieri, A., Tessier, E., Barre, J., Bérail, S., Pedrero, Z., Cherel, Y., Bustamante, P., 2018b. Seabird Tissues As Efficient Biomonitoring Tools for Hg Isotopic Investigations: Implications of Using Blood and Feathers from Chicks and Adults. Environ. Sci. Technol. 52, 4227–4234. https://doi.org/10.1021/acs.est.8b00422

Rodary, D., Bonneau, W., Le Maho, Y., Bost, C.A., 2000a. Benthic diving in male emperor penguins Aptenodytes forsteri foraging in winter. Mar. Ecol. Prog. Ser. 207, 171–181. https://doi.org/10.3354/meps207171

Rodary, D., Wienecke, B.C., Bost, C. a., 2000b. Diving behaviour of Adelie penguins (Pygoscelis adeliae) at Dumont D'Urville, Antarctica: nocturnal patterns of diving and rapid adaptations to changes in sea-ice condition. Polar Biol. 23, 113–120. https://doi.org/10.1007/s003000050016

Rolison, J.M., Landing, W.M., Luke, W., Cohen, M., Salters, V.J.M., 2013. Isotopic composition of species-specific atmospheric Hg in a coastal environment. Chem. Geol. 336, 37–49. https://doi.org/10.1016/j.chemgeo.2012.10.007

Senn, D.B., Chesney, E.J., Blum, J.D., Bank, M.S., Maage, A., Shine, J.P., 2010. Stable isotope (N, C, Hg) study of methylmercury sources and trophic transfer in the northern Gulf of Mexico. Environ. Sci. Technol. 44, 1630–7. https://doi.org/10.1021/es902361j

Sherman, L.S., Blum, J.D., Douglas, T.A., Steffen, A., 2012. Frost flowers growing in the Arctic ocean-atmosphere-sea ice-snow interface: 2. Mercury exchange between the atmosphere, snow, and frost flowers. J. Geophys. Res. Atmos. 117, 1–10. https://doi.org/10.1029/2011JD016186

Sherman, L.S., Blum, J.D., Johnson, K.P., Keeler, G.J., Barres, J. a., Douglas, T. a., 2010. Mass-independent fractionation of mercury isotopes in Arctic snow driven by sunlight. Nat. Geosci. 3, 173–177. https://doi.org/10.1038/ngeo758

Štrok, M., Baya, P.A., Hintelmann, H., 2015. The mercury isotope composition of Arctic coastal seawater. Comptes Rendus - Geosci. 347, 368–376. https://doi.org/10.1016/j.crte.2015.04.001

Sunderland, E.M., Krabbenhoft, D.P., Moreau, J.W., Strode, S.A., Landing, W.M., 2009. Mercury sources, distribution, and bioavailability in the North Pacific Ocean: Insights from data and models. Global Biogeochem. Cycles 23, 1–14. https://doi.org/10.1029/2008GB003425

Thiebot, J., Cherel, Y., Acqueberge, M., Elien, A.U.R., 2014. Adjustment of pre-moult foraging strategies in Macaroni Penguins Eudyptes chrysolophus according to locality, sex and breeding status. Ibis (Lond. 1859). 156, 511–522.

Tremblay, L., Caparros, J., Leblanc, K., Obernosterer, I., 2015. Origin and fate of particulate and dissolved organic matter in a naturally iron-fertilized region of the Southern Ocean. Biogeosciences 12, 607–621. https://doi.org/10.5194/bg-12-607-2015

Tremblay, Y., Cherel, Y., 2003. Geographic variation in the foraging behaviour, diet and chick growth of rockhopper penguins. Mar. Ecol. Prog. Ser. 251, 279–297. https://doi.org/10.3354/meps251279

Wang, Z., Chen, J., Feng, X., Hintelmann, H., Yuan, S., Cai, H., Huang, Q., Wang, S., Wang, F., 2015. Mass-dependent and mass-independent fractionation of mercury isotopes in precipitation from Guiyang, SW China. Comptes Rendus - Geosci. 347, 358–367. https://doi.org/10.1016/j.crte.2015.02.006

Wienecke, B., Robertson, G., Kirkwood, R., Lawton, K., 2007. Extreme dives by free-ranging emperor penguins. Polar Biol. 30, 133–142. https://doi.org/10.1007/s00300-006-0168-8

Yamakawa, A., Takeuchi, A., Shibata, Y., Berail, S., Donard, O.F.X., 2016. Determination of Hg isotopic compositions in certified reference material NIES No. 13 Human Hair by cold vapor generation multi-collector inductively coupled plasma mass spectrometry. Accredit. Qual. Assur.

Zheng, W., Foucher, D., Hintelmann, H., 2007. Mercury isotope fractionation during volatilization of Hg(0) from solution into the gas phase. J. Anal. At. Spectrom. 22, 1097. https://doi.org/10.1039/b705677j

Zheng, W., Xie, Z., Bergquist, B.A., 2015. Mercury stable isotopes in ornithogenic deposits as tracers of historical cycling of mercury in Ross Sea, Antarctica. Env. Sci Technol 49, 7623–7632. https://doi.org/10.1021/acs.est.5b00523